

# Driven Interface Depinning in a Disordered Medium

Heiko Leschhorn<sup>1 \*</sup>, Thomas Nattermann<sup>1</sup>, Semjon Stepanow<sup>2</sup>, and Lei-Han Tang<sup>1 †</sup>

<sup>1</sup>*Institut für Theoretische Physik, Universität zu Köln, Zùlpicher Str. 77, D-50937 Köln, Germany*

<sup>2</sup>*Fachbereich Physik, Martin-Luther Universität Halle, Friedemann-Bach Platz, D-06108 Halle, Germany*

(September 21, 2021)

## Abstract

The dynamics of a driven interface in a medium with random pinning forces is analyzed. The interface undergoes a depinning transition where the order parameter is the interface velocity  $v$ , which increases as  $v \sim (F - F_c)^\theta$  for driving forces  $F$  close to its threshold value  $F_c$ . We consider a Langevin-type equation which is expected to be valid close to the depinning transition of an interface in a statistically isotropic medium. By a functional renormalization group scheme the critical exponents characterizing the depinning transition are obtained to the first order in  $\epsilon = 4 - D > 0$ , where  $D$  is the interface dimension. The main results were published earlier [T. Nattermann et al., J. Phys. II France **2** (1992) 1483]. Here, we present details of the perturbative calculation and of the derivation of the functional flow equation for the random-force correlator. The fixed point function of the correlator has a cusp singularity which is related to a finite value of the threshold  $F_c$ , similar to the mean field theory. We also present extensive numerical simulations and compare them with our analytical results for the critical exponents. For  $\epsilon = 1$  the numerical and analytical results deviate from each other by only a few percent. The deviations in lower dimensions  $\epsilon = 2, 3$  are larger and suggest that the roughness exponent is somewhat larger than the value  $\zeta = \epsilon/3$  of an interface in thermal equilibrium.

**Keywords:** Disorder, interfaces, nonequilibrium phase transitions

---

\*present address: Theoretische Physik III, Heinrich-Heine-Universität Düsseldorf, Universitätsstr. 1, D-40225 Düsseldorf, Germany

†present address: Department of Physics, Imperial College, 180 Queen's Gate, London SW7 2BZ, UK

## I. INTRODUCTION

The ordering dynamics of an Ising magnet following a quench below the Curie (or Neel) temperature is controlled, to a great extent, by the motion of domain walls [1]. This is believed to be true also for impure ferromagnets, where the impurity may either be nonmagnetic (thus we are speaking of dilution or random-bond disorder) or act as to differentiate energetically the coexisting phases (thus we are speaking of random-field disorder). When the disorder is weak, either in terms of impurity strength or concentration, its effect on the bulk phases is minor (at least well above the lower critical dimension), but the behavior of the interface may be dramatically altered: the interface becomes rough in order to take advantage of the inhomogeneous medium, and consequently (free) energy barriers appear between favorable interface configurations, leading to pinning phenomena and extremely slow activated dynamics.

What happens if we apply an external field  $F$  in favor of one of the coexisting phases? Thermodynamically one phase prevails, but this is achievable only if the interface can get out of its locally favorable configurations. At zero temperature, the expected behavior for the interface velocity  $v$  as a function of the driving force is shown in Fig. 1. When the driving force is weak, the interface may adjust itself locally and settles in a nearby metastable position. Steady interface motion sets in only above a threshold value  $F_c$  for the driving force. At finite temperatures, the transition from a pinned to a moving interface is smeared out by thermally activated motion. At low temperatures the rounding effect is however weak apart from a very small region around the transition.

The  $v$ - $F$  curve shown in Fig. 1 is actually representative of a number of other threshold phenomena in condensed systems. Examples include the electrical transport of charge-density-waves (CDWs) [2–5] and driven flux motion in type-II superconductors [6]. A basic theoretical question in all these cases is whether one can calculate the  $v$ - $F$  curve using a suitable model, which to a large extent involves an estimate for  $F_c$  and a theory for the singular behavior around the transition. The first part has been essentially answered twenty years ago in the pioneering work of Larkin [7]. Progress on the second part has been made only recently [8,9]. The difficulty has to do with the fact that the depinning transition is a nonequilibrium critical phenomenon which involves correlated motion of all parts of the system. As it turns out, the key to the solution lies in properly renormalizing the random-force correlator that characterizes the medium.

The present paper is an extension of an earlier one where the basic procedure and results of a functional renormalization group (RG) treatment of the interface problem were reported [8]. The strategy we followed is very similar to the ones for treating equilibrium critical phenomena: the interface model has an upper critical dimension  $D_c = 4$  above which perturbation theory (expanding around a flat, moving interface) converges at weak disorder. For  $D = 4 - \epsilon < D_c$ , it is possible to transform the perturbation theory into a RG procedure using momentum shell integration, which yields flow equations for the parameters of the model. From the fixed point solution of the flow equations one obtains exponents that characterize the depinning transition. Our main aim here is to present details of the perturbative calculation. We shall also try to clarify the relation between the interface model used in our analysis and those considered by others. Finally, we compare the analytical results

with those from our numerical simulations [10,11] which indicate some discrepancy in lower dimensions.

The paper is organized as follows. In Sec. II we introduce the model and review some of its basic properties, in particular the considerations that lead to the identification of an upper critical dimension and characteristic lengths. Section III contains formulation and results of a perturbation theory. The RG flow equations based on the perturbative calculation are presented in Sec. IV, along with a discussion of fixed point solutions and exponents. In Sec. V we present the results of our numerical study. Conclusions and some of the open problems are discussed in Sec. VI.

## II. THE MODEL AND SOME BASIC PROPERTIES

### A. The model

On a certain coarse-grained level, the motion of an interface in an isotropic, weakly disordered medium in the viscous limit can be described by the following equation for the normal velocity  $v_n(\mathbf{R})$  at a position  $\mathbf{R}$ ,

$$\lambda v_n = 2\gamma H + F + \eta(\mathbf{R}) + \varphi(\mathbf{R}, t). \quad (1)$$

Here  $H$  is the mean curvature of the interface at  $\mathbf{R}$ ,  $F$  is the driving force (which is actually a thermodynamic potential that couples to the order parameter),  $\eta(\mathbf{R})$  is a quenched random force,  $\varphi(\mathbf{R}, t)$  is a thermal noise, and  $\lambda$  and  $\gamma$  are friction (or viscosity) and surface tension coefficients, respectively. Such an equation can be motivated from a Ginzburg-Landau theory for the dynamics of the bulk order parameter [12,13,11]. Here we simply accept (1) as a plausible dynamical model for an interface in a disordered medium that is isotropic in a statistical sense.

We now choose a coordinate system with the  $z$ -axis perpendicular to the average interface orientation and the remaining coordinates forming the  $D$ -dimensional  $\mathbf{x}$ -space parallel to the interface. Ignoring overhangs, the interface position is uniquely specified by a function  $z(\mathbf{x}, t)$ . Then Eq. (1) becomes

$$\frac{\lambda}{\sqrt{g}} \frac{\partial z}{\partial t} = \gamma \nabla \cdot (g^{-1/2} \nabla z) + F + \eta(\mathbf{x}, z) + g^{-1/4} \varphi(\mathbf{x}, t), \quad (2)$$

where  $g = 1 + (\nabla z)^2$ . On sufficiently large scales parallel to the interface, the factors  $g$  on the right-hand-side of (2) can be set to one. The effect of the  $g$  factor on the left-hand-side of (2) is more subtle. When the velocity  $v$  of the interface is finite, an expansion of  $g$  in the height gradient gives rise to a term  $\frac{1}{2}\lambda v (\nabla z)^2$  which changes the asymptotic scaling behavior to that of the Kardar-Parisi-Zhang universality class [14]. This term vanishes as  $v \rightarrow 0$ . Thus we expect an interface model defined by [15–17]

$$\lambda \frac{\partial z}{\partial t} = \gamma \nabla^2 z + F + \eta(\mathbf{x}, z), \quad (3)$$

to have the same critical behavior at the zero temperature depinning transition as (2), provided the gradient of the interface height tends to zero on large scales.

Equation (3) is the final model to be analyzed in this paper. At this point a specification of the random force  $\eta$  is called for. For random-field disorder, one may suppose that  $\eta(\mathbf{x}, z)$  is a gaussian random variable that varies over a distance of order  $a$  (e.g., the typical extension of an impurity). A different situation arises for random-bond disorder, where the random force takes a differential form  $\eta(\mathbf{x}, z) = -\mathbf{n} \cdot \nabla_{\mathbf{R}} V(\mathbf{R}) \simeq -\partial V(\mathbf{x}, z)/\partial z$ , with  $V(\mathbf{R})$  being a random potential correlated over a distance  $a$  and  $\mathbf{n}$  the interface norm. A model for driven CDWs can also be casted in the form (3), with  $z$  being a phase variable and  $\eta(\mathbf{x}, z) = \eta_0 \sin[z - \beta(\mathbf{x})]$ , where the independent random variable is the preferred phase  $\beta(\mathbf{x})$  [3–5]. As far as our analysis goes, the three different situations allow a unified description in terms of the pair correlator of the gaussian random forces,

$$\langle \eta(\mathbf{x}', z') \eta(\mathbf{x}' + \mathbf{x}, z' + z) \rangle = \Delta_{\parallel}(\mathbf{x}) \Delta(z), \quad (4)$$

where, without loss of generality, the mean of  $\eta$  is chosen to be zero. Here and elsewhere  $\langle \cdot \rangle$  denotes average over the disorder distribution. The correlation of  $\eta$  in  $\mathbf{x}$ -space is understood to extend over a distance of the coarse-graining length  $a_{\parallel}$  and its precise form is not important in our analysis. In contrast, the functional form of the random-force correlator in  $z$ -space,  $\Delta(z) = \Delta(-z)$ , turns out to be of crucial importance.

Figure 2 illustrates the appropriate functional forms for  $\Delta(z)$  for the three different cases discussed above. The correlator for the random-field disorder is depicted in Fig. 2a), where  $\Delta(z)$  is a monotonically decreasing function of  $z$  for  $z > 0$  and decays exponentially to zero beyond a distance  $a_{\perp}$ . Figure 2b) shows the correlator for the random-bond disorder, where  $\Delta(z) = -R''(z)$ . Here  $R(z)$  denotes the correlator of the random potential  $V(\mathbf{x}, z)$  in  $z$ -direction, which has the same characteristics as the random force correlator shown in Fig. 2a). For the CDW problem [Fig. 2c)],  $\Delta(z)$  is periodic in  $z$  and in addition the integral of  $\Delta(z)$  over one period is zero.

## B. The upper critical dimension

Suppose we accept (3) as a reasonable model for the driven interface, what can one say about its properties before trying to solve it? Surely enough, one can arrive at an important conclusion on the existence of the depinning transition below a certain critical dimension, and an estimate for the threshold force  $F_c$  in the case of weak disorder, using a simple argument due originally to Larkin [7] and developed in the interface context by Bruinsma and Aeppli [16]. Let us recall the argument below.

We begin with the remark, that a completely flat interface is never pinned. Indeed, the total random force on a piece of a flat interface of extension  $L$  is roughly  $\Delta^{1/2}(0)L^{D/2}$  as follows easily from (4). This has to be compared with the total driving force  $FL^D$ , which will always win for  $L \rightarrow \infty$ .

For a rough interface this estimate is only valid on scales  $L$  at which the typical interface distortion  $h$  is smaller than  $a_{\perp}$  and hence pinning is possible for small  $F$ . However, roughness of the interface will be suppressed by the curvature force  $\gamma h L^{-2+D}$ , which tends to flatten the interface. In  $D > D_c = 4$  dimension the curvature force will always win on sufficiently large length scales. Thus, for very weak disorder,  $\Delta(0) \ll \gamma^2 a_{\parallel}^{D-4} a_{\perp}^2$ , there is no length scale

down to  $a_{\parallel}$  at which the interface is rough and hence there is no pinning  $F_c = 0$ . (Pinning is however possible for larger disorder).

The situation is different for  $D < D_c$ : the pinning forces cannot be balanced by the elastic forces for  $h \leq a_{\perp}$  on length scales larger than the Larkin length [7,16],

$$L_c = [\gamma^2 a_{\perp}^2 / \Delta(0)]^{1/\epsilon}, \quad (5)$$

where  $\epsilon = 4 - D$ . Beyond this length, the rough interface explores the random environment to acquire a finite pinning force per unit area. The force that is needed to get the interface out of a typical pinned configuration is thus of the order of [15,16]

$$F_c \simeq \Delta^{1/2}(0) L_c^{-D/2} \sim \Delta^{2/\epsilon}(0). \quad (6)$$

### C. The depinning transition and scaling

The argument presented above suggests that, below the critical dimension  $D_c = 4$ , there is a depinning transition at a finite strength of the driving force. An observation due to Middleton [18], originally made in the CDW context, makes it plausible that  $v$  is a continuous function of  $F$ . Thus the transition, if it exists, should be continuous and the interface is expected to exhibit critical fluctuations at the transition and crossovers away from the transition [8].

We discussed already, that the interface is rough. In particular, we will assume, that the interface is self-affine, an assumption which has to be proven afterwards. In the thermodynamic limit the height correlation function is assumed to obey the following scaling form

$$\langle [z(\mathbf{x}, t) - z(\mathbf{x}', t')]^2 \rangle \sim |\mathbf{x} - \mathbf{x}'|^{2\zeta} G\left(\frac{t - t'}{|\mathbf{x} - \mathbf{x}'|^z}\right), \quad (7)$$

with  $G(y) \rightarrow \text{const}$  for  $y \rightarrow 0$  and

$$G(y) \sim y^{2\zeta/z}, \quad y \rightarrow \infty, \quad (8)$$

where  $\zeta$  and  $z$  (not to be confused with the interface height) are roughness and dynamic exponents, respectively.

For  $F > F_c$  there is a length (and correspondingly, time) scale, above which one can neglect the non-linearity of Eq. (3), which is hidden in the random force term. Going over to a co-moving frame  $z = vt + h(\mathbf{x}, t)$ , where  $v$  is the mean interface velocity and  $\langle h(\mathbf{x}, t) \rangle = 0$ , we consider first the case of high velocity. Then  $\eta(\mathbf{x}, z)$  can be replaced by  $\eta(\mathbf{x}, vt)$ , i.e.  $\eta$  acts as a thermal noise. In this case the exponents are  $z = 2$  and  $\zeta = 0$  for  $D > 2$  and  $\zeta = \frac{2-D}{2}$  for  $D < 2$  [19]. Upon decreasing  $v$ , the non-linearity becomes more important. Indeed, if a small part of the interface hits an obstacle, it will first keep its position, i.e.  $h(\mathbf{x}, t)$  in the argument of  $\eta(\mathbf{x}, vt + h)$  will decrease by  $-\Delta h$  from its original value to compensate the increase of  $vt$ .

The typical value of  $|\Delta h|$  increases with  $t$  according to (7) and (8) as  $t^{\zeta/z}$ . Since  $\zeta < 1$  for a well defined interface and  $z \geq 1$  (as we will show below),  $h$  changes more slowly than  $vt$  and there is a timescale  $t_x \sim v^{-z/(z-\zeta)}$  where the  $vt$  term starts to dominate the argument of  $\eta$ . On this time scale, the perturbation of the interface by the obstacle has spread over a region of linear size

$$\xi \sim v^{-\frac{1}{z-\zeta}}. \quad (9)$$

For larger time or length scales the effect of the non-linearity can be neglected and the above mentioned exponents apply. For smaller scales however, we expect new exponents dominated by the non-linear terms of (3). If the velocity decreases close to the threshold as a power law

$$v \simeq (F - F_c)^\theta, \quad (10)$$

we get  $\xi \simeq (F - F_c)^{-\nu}$  with [8]

$$\theta = \nu(z - \zeta). \quad (11)$$

Another important constraint on the exponents follows from a Harris type argument [20] for a homogeneous transition in a disordered medium: Indeed, let us divide the volume which includes the interface into correlated regions, each of linear size  $\xi$  parallel and  $\xi^\zeta$  perpendicular to the interface, respectively. The typical fluctuation  $\delta F_c$  of the threshold force  $F_c$  in such a region is

$$\delta F_c \sim F_c / \xi^{(D+\zeta)/2}. \quad (12)$$

To have a sharp transition, the condition  $\delta F_c \ll F - F_c$  for  $F \rightarrow F_c$  has to be fulfilled. This gives, together with (12),

$$1/\nu \leq (D + \zeta)/2. \quad (13)$$

#### D. Mean field theory

Above the upper critical dimension  $D_c = 4$ , the dimensional analysis of Sec. II.B suggests absence of a depinning threshold when the disorder is sufficiently weak. This conclusion can be verified explicitly using a perturbation theory discussed in the next section, provided  $\eta(\mathbf{x}, z)$  is differentiable in  $z$ . An exception is given by the case where  $\eta(\mathbf{x}, z)$  may increase abruptly as  $z$  increases (i.e., the pinning force weakens in a discontinuous way), leading to a sudden release of an interface segment. As the phenomenon has an analogy to avalanche motion in lower dimensions, let us discuss it in some detail below.

For simplicity, let us consider a mean field approximation to Eq. (3), which can be obtained by taking the limit of infinite-range, suitably normalized elastic interactions or  $D \rightarrow \infty$ . Then, all interface elements  $z(\mathbf{x}, t)$  are uniformly coupled to the spatially averaged

position  $\bar{z}(t)$  instead of a coupling between nearest neighbors as in Eq. (3). Assuming that the mean position  $\bar{z}(t)$  moves with a constant velocity  $v$ , i.e.  $\bar{z}(t) = vt$ , one obtains [4,17,21],

$$\frac{\partial z}{\partial t} = \tilde{\gamma}[vt - z(t)] + F + \eta(z), \quad (14)$$

where we have omitted the redundant  $\mathbf{x}$ -dependence of  $\eta$  and set  $\lambda = 1$ .

Equation (14) acquires a more transparent form [22] under a new variable  $u \equiv z - vt - (F - v)/\tilde{\gamma}$  which satisfies (upon a translation of  $\eta$ ),

$$\dot{u} = -\tilde{\gamma}u + \eta(vt + u), \quad (15)$$

with the self-consistency condition

$$\tilde{\gamma}\langle u \rangle = -F + v. \quad (16)$$

The driving force  $F$  now disappears from the equation of motion (15) and can be computed from (16) as a function of  $v$  once a solution to (15) is found.

The variable  $u(t)$  in Eq. (15) can be interpreted as the position of an overdamped particle in a moving potential,

$$W(u, t) = \frac{\tilde{\gamma}}{2}u^2 + U(vt + u). \quad (17)$$

The random part  $U(vt + u) = -\int_{z_0}^{vt+u} dz \eta(z)$  travels at a constant velocity  $v$  to the left or to the right depending on the sign of  $v$ .

Using the overdamped particle language, one can relate the threshold force to certain geometrical properties of  $\eta$  without an explicit solution of Eq. (15). Let us define a threshold force for forward motion,  $F_c^{(+)} = \lim_{v \rightarrow 0^+} F(v)$  and a threshold force for backward motion,  $F_c^{(-)} = \lim_{v \rightarrow 0^-} F(v)$ . For a random force with a statistical inversion symmetry [i.e.  $\eta(z) \rightarrow -\eta(-z)$ ],  $F_c^{(+)} = -F_c^{(-)} \equiv F_c$  and Eq. (16) yields [22]

$$F_c = \frac{\tilde{\gamma}}{2} \left[ \lim_{v \rightarrow 0^-} \langle u \rangle - \lim_{v \rightarrow 0^+} \langle u \rangle \right]. \quad (18)$$

Fisher [4] observed that, in the limit  $v \rightarrow 0$ , the particle stays in a local minimum of the potential  $W$  essentially the whole time, interrupted by occasional jumps when the minimum it follows disappears. When the potential travels to the left ( $v > 0$ ), the particle traces the leftmost minimum of  $W$  (apart from an initial transient). The opposite occurs when the potential travels to the right. Thus  $F_c$  is simply proportional to the average distance between the left and right local minima of the potential  $W$ . For a continuous, slow-varying function  $\eta(z)$  with a sufficiently small amplitude, the potential  $W$  has a unique minimum all the time, and hence  $F_c = 0$ . However, for a discontinuous function  $\eta(z)$  (or for sufficiently strong disorder), the potential  $W$  has, from time to time, more than one minimum, and hence a nonvanishing  $F_c$ . Note that only upward jumps in  $\eta$  give rise to upward cusps in the potential which, at times, serve to break one minimum into two.

The different roles played by upward and downward discontinuities of  $\eta$  when the velocity of the particle is small can be appreciated by considering a simple, “two-state” model, which

has been solved explicitly [21]. In this model, the  $z$ -axis is divided into a uniform sequence of cells, each of length  $a$ . The pinning force  $\eta(z)$  is constant in each cell:  $\eta = \pm\eta_0$  with equal probability. Both upward and downward discontinuities are thus present. When the particle encounters a downward discontinuity, it sticks at the cell boundary until the pulling force [including the  $vt$ -term in Eq. (14)] builds up to overtake the resisting force  $-\eta_0$  in the cell ahead, and then enters the new cell at a velocity of the order of  $v$ . The situation is different at an upward discontinuity. When the particle reaches such a point, it suddenly experiences a pulling force by an amount  $2\eta_0$  greater, so that its velocity jumps by the same amount [see Eq. (15)]. This relatively fast motion makes it possible for the particle to sample the negative parts of  $\eta$  more often than the positive parts in the limit  $v \rightarrow 0$ , giving rise to a finite  $F_c$ . At sufficiently small  $\eta_0$  (i.e., no more than two minima occurs at any given time),  $W$  has two minima when the upward discontinuity is within a distance  $\eta_0/\tilde{\gamma}$  from the origin. The distance between the two minima is given by  $\Delta u = 2\eta_0/\tilde{\gamma}$ . Using Eq. (18), one finds  $F_c = \eta_0^2/(2a\tilde{\gamma})$ . Apart from the fast motion (i.e. a sort of instability) caused by the sudden increase of driving at an upward discontinuity of  $\eta$ , the rest of the motion is regular and linear response theory applies. Hence for  $F$  greater than but close to  $F_c$  one expects  $v \sim F - F_c$ . The mean-field velocity exponent is thus given by  $\theta_{\text{MF}} = 1$ . The above results for the threshold and for  $\theta_{\text{MF}}$  are in agreement with the explicit solution of the model [21].

It is interesting to see that a perturbative treatment of Eq. (14) [17] also yields the mean-field exponent  $\theta_{\text{MF}} = 1$ , although, for the “two-state” model, it yields a threshold which is off by a factor of 2. In the lowest order perturbation theory, the disorder is completely specified by its correlator  $\Delta(z)$ . The result for the threshold is given by,

$$F_c \simeq -\Delta'(0^+)/\tilde{\gamma} + O(\Delta^2), \quad (19)$$

i.e., for weak disorder, a finite threshold requires a cusp singularity of the random-force correlator at distance  $0^+$ . For the two-state model,  $\Delta(z) = \eta_0^2(1 - |z|/a)$  for  $|z| < a$  and  $\Delta(z) = 0$ . Both upward and downward discontinuities of  $\eta$  contribute to a nonzero  $\Delta'(0^+) = -\eta_0^2/a$ .

What can we learn from the above discussion for the case  $D < D_c$ , for which the scaling arguments suggest a finite threshold? We have seen that for  $v \rightarrow 0$  the particle  $z(t)$  in mean field theory follows most of the time the minimum of its local potential. The same is true for an interface element  $z(\mathbf{x}, t)$  for  $D < D_c$ . The long periods of slow motion of  $z(\mathbf{x}, t)$  are interrupted when the local minimum disappears. This happens when elastic forces pull the interface element over a barrier of negative  $\eta$ 's. Then the interface element rapidly moves forward and it can itself pull neighboring interface elements over their barriers (“avalanche”). In mean field theory the analogous scenario is when the particle  $z(t)$  is dragged by the mean position  $\bar{z}(t) = vt$  over an upward discontinuity of the random force. The following rapid motion of the particle (“jump”) results in a finite threshold  $F_c > 0$ . The jumps and the finite threshold are a consequence of the discontinuity in  $\eta(z)$ , which correspond to a cusp of the correlator (see Eq. (19)). Given the observation that the jumps (and a finite threshold) are present for  $D < D_c$ , one can expect that this jerky motion has to be described by an *effective* singular correlator  $\Delta(z)$ . In other words, the avalanche-like behavior for  $D < D_c$  can be a mechanism that gives rise to an effective discontinuous random force acting on the interface. We will see below in the functional RG treatment, that the fixed point function



of  $\Delta(z)$  has indeed a cusp singularity at the origin, and that this cusp is responsible for a finite threshold, as in mean field theory [23] !

### III. PERTURBATION THEORY

#### A. Iteration scheme

In this section we present a perturbation theory which forms the basis of our renormalization group calculation.

In the moving phase the interface fluctuates around its average position  $vt$ ,  $z(\mathbf{x}, t) = vt + h(\mathbf{x}, t)$ . Then, Eq. (3) can be written as

$$\lambda \frac{\partial h}{\partial t} = \gamma \nabla^2 h + F - \lambda v + \eta(\mathbf{x}, vt + h(\mathbf{x}, t)). \quad (20)$$

A perturbative solution to Eq. (20) can be found by expanding  $\eta(\mathbf{x}, z)$  around the flat co-moving reference interface  $vt$ . To do so we Fourier-transform  $\eta(\mathbf{x}, vt + h(\mathbf{x}, t))$  with respect to its second argument and expand the term  $e^{iqh}$ ,

$$\begin{aligned} \eta(\mathbf{x}, vt + h(\mathbf{x}, t)) &= \int_q \eta(\mathbf{x}, q) e^{iq[vt+h(\mathbf{x}, t)]} \\ &= \int_q \eta(\mathbf{x}, q) e^{iqvt} \left( 1 + iqh(\mathbf{x}, t) + \frac{1}{2}(iq)^2 [h(\mathbf{x}, t)]^2 + \dots \right), \end{aligned} \quad (21)$$

where  $\int_{-\infty}^{\infty} dq/(2\pi)$  is abbreviated by  $\int_q$ . Since the strength of the disorder  $\Delta(0)$  determines the amplitude of the height fluctuations  $h$ , one expects that the expansion in powers of  $h$  converges for sufficiently weak disorder.

Using (21), we can rewrite (20) in Fourier space,

$$\begin{aligned} \tilde{h}(\mathbf{k}, \omega) &= \tilde{G}_0(\mathbf{k}, \omega) \left\{ \delta(\mathbf{k})\delta(\omega) [F - \lambda v] + \frac{1}{v} \tilde{\eta} \left( \mathbf{k}, \frac{\omega}{v} \right) + \tilde{\varphi}(\mathbf{k}, \omega) \right. \\ &\quad \left. + \int_q \int_{\mathbf{p}} iq \tilde{\eta}(\mathbf{k} - \mathbf{p}, q) \tilde{h}(\mathbf{p}, \omega - qv) \right. \\ &\quad \left. + \frac{1}{2} \int_q \int_{\mathbf{p}} \int_{\Omega} \int_{\mathbf{p}'} (iq)^2 \tilde{\eta}(\mathbf{k} - \mathbf{p} - \mathbf{p}', q) \tilde{h}(\mathbf{p}, \Omega) \tilde{h}(\mathbf{p}', \omega - \Omega - qv) + \dots \right\}. \end{aligned} \quad (22)$$

Here,  $\int_{\mathbf{p}} \equiv \int d^D p / (2\pi)^D$  and the bare propagator is defined by

$$\tilde{G}_0(\mathbf{k}, \omega) = \frac{1}{\gamma k^2 + i\lambda\omega}. \quad (23)$$

We added a source term  $\tilde{\varphi}(\mathbf{k}, \omega)$  on the *rhs* of Eq. (22). The Fourier-transformed quantities, e.g.,

$$\tilde{h}(\mathbf{k}, \omega) = \int d^D x dt h(\mathbf{x}, t) e^{-i(\mathbf{k} \cdot \mathbf{x} + \omega t)}, \quad (24)$$

are marked by a tilde. Eq. (22) can be represented diagrammatically, as shown in Fig. 3. The short double arrow represents  $\tilde{h}$ , a line with an arrow is the bare propagator  $\tilde{G}_0(\mathbf{k}, \omega)$ , a cross  $\times$  stand for  $\delta(\mathbf{k})\delta(\omega) [F - \lambda v]$  and the open circle denotes the source term  $\tilde{\varphi}$ . A filled circle with a dotted line indicates the quenched noise  $\eta$ , where the number of outgoing arrows of such a vertex determines the power of the term  $iq$  and the number of  $D + 1$  dimensional integrations.

The averaging over the quenched noise will be represented by the connection of two dotted lines and is performed using

$$\langle \tilde{\eta}(\mathbf{k}, q) \tilde{\eta}(\mathbf{k}', q') \rangle = \tilde{\Delta}_{\parallel}(\mathbf{k}) \Delta_q \delta^D(\mathbf{k} + \mathbf{k}') \delta(q + q'), \quad (25)$$

where  $\tilde{\Delta}_{\parallel}(\mathbf{k}) \simeq e^{-a_{\parallel}^2 \mathbf{k}^2}$  is the Fourier transform of  $\Delta_{\parallel}(\mathbf{x})$  and  $\Delta_q$  is defined by

$$\Delta(z) = \int_q \Delta_q e^{iqz}. \quad (26)$$

Assuming  $\Delta(z)$  is analytic at  $z = 0$ , we may write

$$\Delta(z) = \sum_{n=0}^{\infty} \frac{(-1)^n}{(2n)!} z^{2n} Q_{2n}, \quad (27)$$

where

$$Q_{2n} \equiv \int_q q^{2n} \Delta_q \quad (28)$$

will be called moments of the noise correlator  $\Delta$ .

Equation (22) can now be solved by iteration. As an example, we insert the second term  $\tilde{G}_0 v^{-1} \tilde{\eta}$  on the *rhs* of Eq. (22) for the  $\tilde{h}$  of the fourth term which gives a “one-loop” contribution to the solution  $\tilde{h}(\mathbf{k}, \omega)$ . Neglecting higher order terms and averaging Eq. (22) over the disorder, we obtain (see Fig. 4)

$$v \simeq \frac{1}{\lambda} F + \frac{1}{\lambda} \int_q \int_{\mathbf{p}} \frac{iq \Delta_q}{\gamma \mathbf{p}^2 - i\lambda v q}. \quad (29)$$

For  $D > D_c = 4$ , the integral in the correction term converges for all  $v$  (see Appendix A.1).

When  $D < 4$ , the integral in (29) diverges in the limit  $v \rightarrow 0$  due to contributions from small momenta,  $p \rightarrow 0$  (see Appendix A.1). This statement can be confirmed by continuing the iteration to higher orders (see Appendix A.2). Quite generally, the expansion parameter can be written in the form  $(\xi_0/L_c)^{4-D}$ , where

$$\xi_0 = (\gamma a_{\perp} / \lambda v)^{1/2} \quad (30)$$

plays the role of a bare correlation length. This parameter is small at high velocities.

## B. Linear response and renormalization of $\gamma$ and $\lambda$

In the moving phase, the interface is free on large length and time scales. The dynamics of the system for small  $k$  can thus be described by linear response theory with effective parameters. As usual, one can define an effective linear response function  $\tilde{G}(\mathbf{k}, \omega)$  [24],

$$\tilde{G}(\mathbf{k}, \omega) = \left. \frac{\partial \tilde{h}(\mathbf{k}, \omega)}{\partial \tilde{\varphi}(\mathbf{k}, \omega)} \right|_{\tilde{\varphi}=0}. \quad (31)$$

Due to the nonlinear terms in Eq. (22),  $\tilde{G}(\mathbf{k}, \omega)$  differs from  $\tilde{G}_0(\mathbf{k}, \omega)$ . The correction can be expressed in terms of a “self-energy”  $\tilde{\Sigma}(\mathbf{k}, \omega)$ ,

$$\tilde{G}(\mathbf{k}, \omega) = \tilde{G}_0(\mathbf{k}, \omega) + \tilde{G}_0(\mathbf{k}, \omega) \tilde{\Sigma}(\mathbf{k}, \omega) \tilde{G}(\mathbf{k}, \omega). \quad (32)$$

As we shall show,  $\tilde{\Sigma}(\mathbf{k}, \omega)$  has the same functional form as  $\tilde{G}_0^{-1}(\mathbf{k}, \omega)$  at small  $\mathbf{k}$  and  $\omega$ . Hence the correction term in (32) can be absorbed into the free one with the bare parameters  $\gamma$  and  $\lambda$  replaced by effective parameters  $\lambda_{eff} = \lambda + \delta\lambda$  and  $\gamma_{eff} = \gamma + \delta\gamma$ .

To calculate  $\delta\gamma$  and  $\delta\lambda$  one has to consider diagrams with one incoming and one outgoing line (see Eq. (32)). The lowest order contribution to the self energy  $\tilde{\Sigma}(\mathbf{k}, \omega)$  is given by the second and third diagram on the *rhs* of the diagrammatic perturbation expansion for  $\tilde{G}(\mathbf{k}, \omega)$  shown in Fig. 5. The corresponding analytic expression is

$$\tilde{\Sigma}(\mathbf{k}, \omega) \simeq \int_q \int_{\mathbf{p}} \Delta_q \left\{ \frac{(iq)^2}{\gamma \mathbf{p}^2 + i\lambda qv} - \frac{(iq)^2}{\gamma (\mathbf{p} + \mathbf{k})^2 + i\lambda(\omega + qv)} \right\}. \quad (33)$$

For small  $\mathbf{k}$  and  $\omega$  Eq. (33) can be written as

$$\tilde{\Sigma}(\mathbf{k}, \omega) \simeq \left[ \gamma \mathbf{k}^2 \left( \frac{4}{D} - 1 \right) - i\lambda\omega \right] \int_q \int_{\mathbf{p}} \frac{q^2 \Delta_q}{(\gamma \mathbf{p}^2 + i\lambda vq)^2}. \quad (34)$$

As in Eq. (29), the integration over  $p$  converges at large  $p$  as long as  $4 - D = \epsilon > 0$ , while  $\sqrt{\lambda v q / \gamma}$  serves as a lower cutoff for  $p$ . The  $q$  integration is truncated for large  $q$  by the correlator  $\Delta_q$  which is assumed to decay as  $e^{-q^2 a_\perp^2}$ . The integrals can be evaluated to give

$$\tilde{\Sigma}(\mathbf{k}, \omega) \simeq Q_2 \frac{K_D}{\gamma^2} \frac{1}{\epsilon} \left( \frac{\gamma a_\perp}{\lambda v} \right)^{\epsilon/2} \left[ \gamma \frac{\epsilon}{D} \mathbf{k}^2 - i\lambda\omega \right] \quad (35)$$

(see Appendix A.1, where similar integrals are carried out). When comparing this with Eq. (23) and using (32), the first order corrections  $\delta\gamma^{(1)}$  and  $\delta\lambda^{(1)}$  to  $\gamma$  and  $\lambda$  are [25]

$$\delta\gamma^{(1)} = -\gamma c Q_2 \frac{1}{D} \xi_0^\epsilon \equiv -\gamma \frac{K_D}{D} \left( \frac{\xi_0}{L_c} \right)^\epsilon, \quad (36)$$

$$\delta\lambda^{(1)} = \lambda c Q_2 \frac{1}{\epsilon} \xi_0^\epsilon = \lambda \frac{K_D}{\epsilon} \left( \frac{\xi_0}{L_c} \right)^\epsilon, \quad (37)$$

where  $c \equiv K_D / \gamma^2$  and  $L_c^\epsilon = \gamma^2 / Q_2$ . With these notations the small parameter of the perturbation theory can be written as  $c Q_2 \xi_0^\epsilon$  or as  $(\xi_0 / L_c)^\epsilon$ . We see that  $Q_2 = -\Delta''(0)$  plays the role of a coupling constant.

The result for  $\delta\lambda^{(1)}$  in (37) can also be obtained by considering the lowest order correction Eq. (29) to the bare velocity  $v_0 = F/\lambda$ , as done by Feigel'man [15]. In Appendix A.2 the calculation of the velocity is extended to second order, with the result,

$$\lambda_{eff} = \lambda \left[ 1 + \frac{\delta\lambda^{(1)}}{\lambda} + \left( \frac{\delta\lambda^{(1)}}{\lambda} \right)^2 + \dots \right]. \quad (38)$$

The series obtained by perturbation theory are thus divergent for  $v \rightarrow 0$  and cannot be used directly close to the depinning transition.

### C. Interface width

The width of the interface  $\langle h^2(\mathbf{x}, t) \rangle$  can be calculated from Eq. (22) in a very similar way as the velocity. The lowest order diagram for the width is shown in Fig. 6. The corresponding analytical expression is given by

$$\langle h^2(\mathbf{x}, t) \rangle = \int_q \int_{\mathbf{p}} \Delta_q \frac{1}{\gamma^2 \mathbf{p}^4 + (\lambda v q)^2} \quad (39)$$

which can be evaluated easily, giving

$$\begin{aligned} \langle h^2(\mathbf{x}, t) \rangle &\simeq a_{\perp}^2 \frac{2K_D}{D-2} \frac{1}{\epsilon} \frac{\Delta(0)}{a_{\perp}^2 \gamma^2} \left( \frac{a_{\perp} \gamma}{\lambda v} \right)^{\epsilon/2} + O(\epsilon) \\ &\simeq a_{\perp}^2 \frac{2K_D}{D-2} \frac{1}{\epsilon} \left( \frac{\xi_0}{L_c} \right)^{\epsilon} + O(\epsilon). \end{aligned} \quad (40)$$

The interface width diverges with  $v \rightarrow 0$ . Since  $\xi_0$  is a correlation length, one obtains from Eq. (40) the perturbative roughness exponent  $\zeta_p = \epsilon/2$ .

It can be shown that the second order contribution to  $\langle h^2(\mathbf{x}, t) \rangle$  is proportional to the square of the first order Eq. (40) but with one factor  $1/\epsilon$  lacking:

$$a_{\perp}^2 \left( \frac{2K_D}{D-2} \right)^2 \frac{1}{\epsilon} \left( \frac{\xi_0}{L_c} \right)^{2\epsilon}. \quad (41)$$

Here we have implicitly assumed that  $\Delta'(0) = 0$  which will be discussed below (Sec. V.).

### D. Renormalization of the moments of $\Delta(z)$

In the preceding section we have considered the renormalization of  $\gamma$  and  $\lambda$ . Eqs. (36-37) show that the parameter controlling the renormalization of  $\lambda$  is proportional to the second moment of the disorder correlator  $Q_2 = \int_q q^2 \Delta_q$ . In order to carry out the renormalization group analysis of the problem it is necessary to know the renormalization prescription of  $Q_2$ . The usual way to get this prescription is to find a vertex function, which is proportional to  $Q_2$  when calculating the lowest-order contribution in the disorder strength. Then, the higher-order contributions to this vertex function yield the desired renormalization prescription of  $Q_2$ . It turns out that a convenient quantity to look at for this purpose is

$$G_{11} = \int_{\Omega_1} \int_{\Omega'_1} \tilde{G}_0^{-1}(\mathbf{k}, \omega) \tilde{G}_0^{-1}(\mathbf{k}', \omega') \times \left\langle \frac{\delta \tilde{h}(\mathbf{k}, \omega)}{\delta \tilde{h}_0(\mathbf{p}_1, \Omega_1)} \bigg|_{\substack{\tilde{h}_0=0, \omega=0 \\ \mathbf{k}=\mathbf{p}_1=0}} \frac{\delta \tilde{h}(\mathbf{k}', \omega')}{\delta \tilde{h}_0(\mathbf{p}'_1, \Omega'_1)} \bigg|_{\substack{\tilde{h}_0=0, \omega'=0 \\ \mathbf{k}'=\mathbf{p}'_1=0}} \right\rangle_c, \quad (42)$$

where  $\tilde{h}_0(\mathbf{p}, \Omega) = \tilde{G}_0(\mathbf{p}, \Omega) \tilde{\varphi}(\mathbf{p}, \Omega)$ . The subscript  $c$  indicates that only connected diagrams are to be considered. The perturbation expansion of (42) in powers of the disorder correlator is obtained by iterating  $\tilde{h}(\mathbf{k}, \omega)$  in Eq. (42) according to Eq. (22) and carrying out the average over the disorder. This perturbation expansion can be represented by means of diagrams. The lowest order contribution to (42) in powers of  $\Delta(z)$  is found by replacing all  $\tilde{h}$  on the *rhs* of Eq. (22) by  $\tilde{h}_0$ . The first-order contribution to (42) is given by diagram a) in Fig. 7 with  $n = 1$ . According to Eq. (42) and Eq. (22) the analytical expression associated with the diagram 7a) is exactly the second moment  $Q_2$ . The renormalization prescription of  $Q_2$  can be obtained from the one-loop diagrams in Fig. 7b)-d) by setting  $n = 1$ . In each of these diagrams, there is only one integration over the internal momentum  $\mathbf{p}$ . This integration has the form  $\int_{\mathbf{p}} G_0^2(\mathbf{p})$  and yields for all diagrams under consideration the same factor  $c\xi_0^\epsilon/\epsilon$ . In addition to this integration, there is also a factor which involves an integration over the momenta  $q_1$  and  $q_2$  conjugated to the argument of the disorder correlator  $\Delta(z)$ . This factor results in

$$\int_{q_1} \int_{q_2} (-q_1 q_2^3 + 3q_1^2 q_2^2 - 3q_1^3 q_2) \Delta(q_1) \Delta(q_2) = 3Q_2^2, \quad (43)$$

where we have taken into account that only even moments of the disorder correlator differ from zero. The total contribution of the diagrams in Fig. 7 for  $n = 1$  leads to the following renormalization prescription of  $Q_2$ ,

$$Q_{2,eff} = Q_2(1 + 3Q_2 c \frac{1}{\epsilon} \xi_0^\epsilon + \dots). \quad (44)$$

A detailed analysis of the present problem shows that, besides the renormalization of the second moment, higher moments  $Q_{2n}$  ( $n = 2, \dots$ ) also renormalize. The renormalization of  $Q_{2n}$  can be derived by considering the following generalization of the expression (42),

$$G_{nn} = \int_{\Omega_1} \int_{\Omega'_1} \tilde{G}_0^{-1}(\mathbf{k}, \omega) \tilde{G}_0^{-1}(\mathbf{k}', \omega') \times \left\langle \frac{\delta^n \tilde{h}(\mathbf{k}, \omega)}{\delta \tilde{h}_0(\mathbf{p}_1, \Omega_1) \delta \tilde{h}_0(\mathbf{p}_2, \Omega_2) \cdots \delta \tilde{h}_0(\mathbf{p}_n, \Omega_n)} \bigg|_{\substack{\tilde{h}_0=0, \omega=\Omega_2=\dots=\Omega_n=0 \\ \mathbf{k}=\mathbf{p}_1=\dots=\mathbf{p}_n=0}} \frac{\delta^n \tilde{h}(\mathbf{k}', \omega')}{\delta \tilde{h}_0(\mathbf{p}'_1, \Omega'_1) \delta \tilde{h}_0(\mathbf{p}'_2, \Omega'_2) \cdots \delta \tilde{h}_0(\mathbf{p}'_n, \Omega'_n)} \bigg|_{\substack{\tilde{h}_0=0, \omega'=\Omega'_2=\dots=\Omega'_n=0 \\ \mathbf{k}'=\mathbf{p}'_1=\dots=\mathbf{p}'_n=0}} \right\rangle_c. \quad (45)$$

The perturbation expansion of (45) is obtained in the same way as the iteration of Eq. (42). The lowest-order contribution to (45) in powers of  $\Delta(z)$  is found by replacing all  $\tilde{h}$  on the *rhs* of Eq. (22) by  $\tilde{h}_0$ . Only the diagram with  $n$  outgoing lines and one dotted line in Fig. 3 gives a contribution to the first-order correction of  $G_{nn}$ . As it can be easily shown, the

latter is equal to the bare moment  $Q_{2n}$  (see Eq. (27)) and is represented by the diagram a) in Fig. 7. The second-order contributions to  $G_{nn}$  in powers of  $\Delta$  are given by diagrams b)-d) in Fig. 7. The renormalization of the moments  $Q_{2n}$  and consequently the renormalization of the disorder correlator  $\Delta(z)$ , can be obtained by computing  $G_{nn}$  up to the second order in  $\Delta$ . The details of such one-loop computation of  $G_{nn}$  are presented in Appendix B. As a result, the renormalization prescription of the moments  $Q_{2n}$  is obtained as

$$Q_{2n,eff} - Q_{2n} \simeq \delta Q_{2n}^{(1)} \simeq \sum_{k=1}^n C_{2k}^{2n+1} Q_{2k} Q_{2n-2k+2} \frac{c}{\epsilon} \xi_0^\epsilon, \quad (46)$$

where  $C_i^j = \binom{j}{i}$  are the binomial coefficients (see Appendix B). In particular, the correction to the second moment  $Q_2$  is given by Eq. (44). Eq. (46) has been derived for  $n = 1, 2, \dots$ . However, it can be extended to  $n = 0$ . Taking into account that  $C_2^1 = 0$  we get from (46) that the zeroth moment  $Q_0$  does not renormalize. This conclusion is in agreement with the result on the interface width in the preceding section. Equation (46) will be used in Sec. IV to derive the flow equation for the correlator  $\Delta(z)$ .

#### IV. RENORMALIZATION GROUP

Approaching the critical point with  $v \rightarrow 0$ , the perturbative corrections to the parameter of the model diverge as  $v^{-\epsilon/2}$ , which is caused by the integration over small momenta. A possible way to sum up such singularities is to perform a renormalization group (RG) procedure, where one integrates out fluctuations in an infinitesimal momentum shell only, leading to differential flow equations. From the flow of the relevant parameters the critical behavior can be deduced. The calculation is simplified close to the upper critical dimension  $D_c = 4$ . We will therefore determine the critical exponents of the depinning transition by a RG procedure in  $D = 4 - \epsilon$  dimensions.

##### A. Three-parameter RG

The smallest closed set of flow equations to first order in  $\epsilon$  is given by [8]

$$d \ln \gamma / d \ln L = 0, \quad (47)$$

$$d \ln \lambda / d \ln L = c Q_2 L^\epsilon, \quad (48)$$

$$d Q_2 / d \ln L = 3 c Q_2^2 L^\epsilon \quad (49)$$

( $c \equiv K_D / \gamma^2$ ). To derive these flow equations we consider  $\gamma_{eff}$ ,  $\lambda_{eff}$  and  $Q_{2,eff}$  as depending on the upper cut-off length,  $L = \xi_0$ . Eqs. (47)-(49) can be formally obtained by differentiating Eqs. (36), (37), and (44) and then setting  $\gamma_{eff} = \gamma$ ,  $\lambda_{eff} = \lambda$ , and  $Q_{2,eff} = Q_2$ . This is equivalent to the RG transformation, where the degrees of freedom in a momentum shell are successively integrated out. There, the corrections to the parameters are calculated in the same way as in perturbation theory - the only difference is that one integrates only over the momentum shell instead over all momenta.

Note that the perturbative correction (36) for  $\gamma$  is *finite* in the limit  $\epsilon \rightarrow 0$  and does not contribute to first order to a renormalization of  $\gamma$  [25]. The flow equation (49) can also be obtained from the second order correction (38) to the velocity [26].

Since there is no  $1/\epsilon^2$  term in the second order correction (41) of the interface width, provided  $\Delta'(0) = 0$ , we conclude that  $\Delta(0)$  does not renormalize to first order in  $\epsilon$ .

When integrating Eq. (49) we see that  $Q_2$  becomes infinite at  $L \simeq L_c$  (if we assume that  $\Delta(z)$  is analytic and monotonously decaying). It then follows from Eq. (48) that also  $\lambda$  diverges at  $L \simeq L_c$ . This means that beyond  $L_c$ , there is no dynamic response to any finite force, which is an unphysical result !

## B. Functional RG

Eq. (46) shows that besides the renormalization of  $Q_2$  there is also a renormalization of all the other moments  $Q_{2n}(n = 2, \dots)$ . The renormalization of the moments causes a renormalization of the disorder correlator  $\Delta(z)$  [26]. Since all  $Q_{2n}$  have the same upper critical dimension we can put together the prescriptions (46) into a functional flow equation [26] for  $\Delta(z)$  (see Appendix C):

$$\frac{d \Delta(z)}{d \ln L} = -cL^\epsilon \frac{d^2}{dz^2} \left[ \frac{1}{2} \Delta^2(z) - \Delta(z)\Delta(0) \right]. \quad (50)$$

To discuss the fixed point behavior it is convenient to consider the renormalized *and* rescaled correlator  $\hat{\Delta}(z)$ , which has the original short-distance cutoff of the bare correlator. To do so we perform a scale transformation  $\mathbf{x} \rightarrow L\mathbf{x}$ ,  $t \rightarrow L^z t$ , and  $h \rightarrow L^\zeta h$  with Eq. (20). At the critical point we expect scale invariance. Since  $\gamma$  is not renormalized, the renormalized and rescaled equation of motion,

$$\lambda L^{2-z} \frac{\partial h}{\partial t} = \gamma \nabla^2 h + L^{2-\zeta} (F - \lambda v) + L^{2-\zeta} \eta(L\mathbf{x}, vL^z t + L^\zeta h), \quad (51)$$

should be independent of  $L$ . This is the case when  $\lambda(L) \sim L^{z-2}$  and

$$\Delta(z) = \text{const.} \times L^{2\zeta-\epsilon} \hat{\Delta}(zL^{-\zeta}). \quad (52)$$

To investigate the fixed point solution  $\Delta^*(y) = \lim_{L \rightarrow \infty} \hat{\Delta}(y)$  we insert (52) into (50), take the limit  $L \rightarrow \infty$ , and determine the constant in Eq. (52) such that  $\Delta^*(0) = 1$ ,

$$(\epsilon - 2\zeta)\Delta^*(y) + \zeta y \Delta^{*'}(y) - [\Delta^{*'}(y)]^2 - \Delta^{*''}(y)[\Delta^*(y) - 1] = 0. \quad (53)$$

The same equation with  $\Delta^*(y) = R^{**}(y)$  was already derived for the potential-potential correlator  $R(y)$  in the problem of an equilibrium interface subject to a random potential [27]. From that treatment it is known [27] that the fixed-point function  $\Delta^*(y)$  has a singularity at the origin. The ansatz

$$\Delta^*(y) = 1 + a_1|y| + \frac{1}{2}a_2y^2 + \dots \quad (54)$$

satisfies Eq. (53) and by a comparison of the coefficients of  $y^0$  and  $y^1$  one gets  $a_1^2 = \epsilon - 2\zeta$  and  $a_2 = (\epsilon - \zeta)/3$ .

The development of this cusp singularity can be understood as follows (see Fig. 8). Starting the renormalization procedure at  $L = L_0$  with a smooth correlator ( $\Delta''(0) < 0$ ), the curvature of  $\Delta(z)$  at the origin becomes greater under the flow (49). Hence, the position  $z_0$  of the point where the second derivative  $\Delta''(z)$  changes its sign is shifted closer to the origin. A diverging curvature means  $z_0 = 0$ , i.e.  $\Delta''(z \rightarrow 0^+) > 0$ .

Repeating the perturbative calculations with a correlator obeying Eq. (54) we find that Eqs. (36), (37) and (47), (48) remain valid to first order in  $\epsilon$ . With the interpretation  $Q_2 = \Delta''(0^+) > 0$  we overcome the above unphysical result that the inverse mobility diverges at  $L = L_c$ .

Since our earlier assumption  $\Delta'(0) = 0$  failed, which yields (41), the conclusion of the nonrenormalization of  $\Delta(0)$  is no longer valid. Instead we obtain with Eq. (54)  $\partial\Delta(0)/\partial\ln L = -cL^\epsilon[\Delta'(0)]^2$  which is in agreement with Eq. (53) for  $y = 0$  when using Eq. (52).

The singular term  $|z|$  yields a reduction of the driving force,  $F \rightarrow F - F_c$ . To see this we split the correlator  $\Delta$  in a regular and a singular part. In Fourier-space, the singular part behaves as  $\Delta_q^{\text{sing}} \sim -q^{-2}\Delta'(z \rightarrow 0^+)$ . Using this in Eq. (29) for the velocity, we obtain

$$F_c \simeq -\frac{K_D}{D-2} \frac{1}{\gamma} \Delta'(L_0, z \rightarrow 0^+) \Lambda_0^{D-2}, \quad (55)$$

which depends on the upper cutoff  $\Lambda_0 \simeq \pi/L_0$  of the momentum space integration. Using  $\Delta'(0^+) = \Delta(0)/a_\perp$  (see Eq. (54)) and identifying  $L_0$  with  $L_c$  yields the threshold  $F_c$  of Eq. (6), in agreement with the estimate of the scaling arguments [7,15,16].

### C. Critical exponents

The roughness exponent  $\zeta$  can be obtained immediately from Eq. (53), provided  $\Delta^*(y)$  goes sufficiently fast to zero with  $y \rightarrow 0$ . Integration over  $y$  yields  $(\epsilon - 3\zeta) \int_{-\infty}^{\infty} dy \Delta^*(y) = 0$ . For random-field disorder  $\int_{-\infty}^{\infty} dy \Delta^*(y) > 0$ , from which one gets

$$\zeta = \epsilon/3. \quad (56)$$

The other exponents can be read off from Eq. (51). To calculate the dynamical exponent  $z$  we have to know the scale dependence of  $\lambda$ , which can be obtained by integrating (48) using (52) and (54),

$$\lambda(L) = \lambda_0(L/L_0)^{-(\epsilon-\zeta)/3}, \quad (57)$$

where  $\lambda_0 = \lambda(L_0)$ . Using Eqs. (4), (52), (57) and imposing scale invariance of Eq. (51) at  $F \rightarrow F - F_c = v = 0$ ,  $z$  is given by

$$z = 2 - (\epsilon - \zeta)/3. \quad (58)$$



As discussed earlier, above the threshold the quenched character of the noise correlator changes to a thermal one on length scales  $L \geq \xi \sim v^{-1/(z-\zeta)}$ . Hence we have to stop the renormalization at  $\xi$ . From  $F - F_c = \lambda(L = \xi)v$  follows

$$v \sim (F - F_c)^\theta, \quad \text{with } \theta = 1 - \frac{1}{3} \frac{\epsilon - \zeta}{2 - \zeta} \quad (59)$$

$$\xi \sim (F - F_c)^{-\nu}, \quad \text{with } \nu = 1/(2 - \zeta) \quad (60)$$

where we have used Eqs. (57) and (58).

Inserting the result for random-field disorder  $\zeta = \epsilon/3$  in Eqs. (58) and (59), (60) we obtain the final results for the critical exponents to first order in  $\epsilon$ ,

$$\begin{aligned} \zeta &\simeq \frac{1}{3}\epsilon, & z &\simeq 2 - \frac{2}{9}\epsilon, \\ \theta &\simeq 1 - \frac{1}{3} \frac{2\epsilon}{6 - \epsilon} \simeq 1 - \frac{1}{9}\epsilon, & \nu &\simeq \frac{3}{6 - \epsilon} \simeq \frac{1}{2} + \frac{1}{12}\epsilon. \end{aligned} \quad (61)$$

The roughness exponent  $\zeta = \epsilon/3 + O(\epsilon^2)$  differs from the value  $\zeta_p = \epsilon/2$  from perturbation theory (see Sec. III. C) [2,28], but coincides with that of an equilibrium interface in a medium with random-field disorder [1]. Recently, Narayan and Fisher [9] showed that higher order terms in Eq. (50) vanish when integrated over all  $z$ . Thus, the results for the exponents  $\zeta$  and  $\nu$  could be exact, although non-perturbative corrections cannot be ruled out [9]. In fact, as we will see in the next section, our simulations in  $D \leq 3$  yield values for  $\zeta$  and  $\nu$  which differ slightly from the results (61).

The velocity exponent  $\theta$  is smaller than one for  $D < 4$  and approaches the mean field value  $\theta_{\text{MF}} = 1$  for  $D = 4$  (see Sec. II). The superdiffusive dynamical exponent  $z < 2$  is consistent with the expectation that the motion of the interface close to threshold is governed by the behavior of avalanches [29]. The Harris condition (13) is fulfilled as an equality to the first order in  $\epsilon$ . Narayan and Fisher [9] showed that the scaling relation (60) between  $\zeta$  and  $\nu$  is exact due to a symmetry of Eq. (3). Thus, the Harris condition (13) can be written as  $\zeta \geq (4 - D)/3$ .

Narayan and Fisher [9] investigated also the RB case (see Sec. II) and argued that the results (61) are also valid for RB disorder. The critical exponents for CDW's can be obtained by inserting the corresponding value  $\zeta_{\text{CDW}} = 0$  into the scaling relations (58), (59) and (60) which are independent of the form of the correlator  $\Delta(z)$  (see Sec II.) [5].

## D. Phase diagram

The crossover behavior of the equation of motion (3) can be summarized in a  $F - L$  phase diagram which is shown in Fig. 9. On small scales  $L < L_c$  the height fluctuations are bounded by the microscopic correlation length  $a_\perp$  of the random forces. Here, the correlations (4) can be described by a smooth function  $\Delta(z)$ . On larger length scales  $L_c < L < \xi$  the system is in a critical state. The behavior of the interface is characterized by the critical exponents of the depinning transition. When crossing the Larkin length  $L_c$ , the second derivative  $\Delta''(0)$  diverges under the RG flow and the fixed-point function  $\Delta^*(z)$  of

the correlator develops a cusp singularity at the origin. When going to length scales larger than  $\xi$  (for  $F > F_c$ ), the behavior crosses over to the EW regime [19]. The full equation of motion (2) has (for  $T = 0$ ) an additional regime, namely the one of the KPZ equation [14]. For  $D > 1$  this regime is situated above the region of the EW equation.

## V. NUMERICAL RESULTS

In this section we compare the analytical results for the critical exponents with extensive numerical simulations [10,11]. Since our analytical values for the exponents (61) have been obtained by an expansion to first order in  $\epsilon$ , it is an open question whether or not the results (61) are applicable to  $\epsilon \geq 1$ . However, further work by Narayan and Fisher [9] suggests that the first-order results for the exponents  $\zeta$  and  $\nu$  are exact. We will see below that this is not consistent with our numerical simulations. The deviations between the analytical results and the simulations are much larger than the error bars on the numerical values but decrease with increasing  $D = 4 - \epsilon$ , thereby supporting our analytical calculation.

### A. Simulation of the continuum equation in $D = 1$

We first simulate Eq. (3) in  $D = 1$  with a discretization of the transverse coordinate only,  $x \rightarrow i$ ,  $z(x, t) \rightarrow z_i(t)$ . The random forces  $\eta_i(z_i)$  are chosen as follows: Each integer position  $z_i$  on a square lattice is assigned a random number  $\eta$  between zero and one. For non-integer  $z_i$  the forces  $\eta_i(z_i)$  are obtained by linear interpolation [28]. Finally, the  $z$ -coordinates of  $\eta_i(z_i)$  in each column  $i$  are shifted by a random amount  $0 \leq s_i < 1$ , i.e.,  $\eta_i(z_i) \rightarrow \eta_i(z_i + s_i)$  [11].

At  $t = 0$  the interface is flat,  $z_i(t = 0) \equiv 0$ . The interface configuration at  $t + \Delta t$  is calculated simultaneously for all  $i$  using the method of finite differences,

$$z_i(t + \Delta t) = z_i(t) + \Delta t [F + z_{i+1}(t) + z_{i-1}(t) - 2z_i(t) + m\eta_i(z_i)]. \quad (62)$$

Here  $m$  is a real parameter and periodic boundary conditions are used.

We are interested in the critical exponents, so the threshold  $F_c$  has to be determined from a measurement of the velocity  $v(F)$  close to  $F_c$  where Eq. (10) is valid. However, it turns out that the critical region is very narrow and that an accurate determination of  $v(F)$  inside that region is difficult, which seems to be the reason for contradictory results for  $\theta$  in the literature [28,30,31]. At the beginning of the interface motion the velocity decreases and only saturates after a time  $t_v$  when the roughness  $w \sim \xi^\zeta$  no longer increases. The time  $t_v$  behaves as  $t_v \sim (F - F_c)^{-z\nu}$  and therefore the simulations become increasingly time-consuming when approaching the threshold. In addition, the average velocity  $v$  is systematically underestimated if the temporal fluctuations of the velocity become comparable with  $v$  itself. Thus, for  $F$  close to  $F_c$  very large systems have to be simulated.

For  $m = 3$  we estimated the threshold to be in the interval  $1.41 \leq F_c \leq 1.42$  and for the velocity exponent we obtained an upper bound,  $\theta(D = 1) \leq 0.45$ .

To determine the roughening exponent  $\beta \equiv \zeta/z$ , we measured the interface width  $w^2(L, t) = \langle [z_i(t) - \bar{z}_i(t)]^2 \rangle$  and the average position  $H(t) \equiv \langle \bar{z}(t) \rangle$  in the transient regime,

$t \ll L^z, \xi^z$  for various forces in the interval  $1.41 \leq F \leq 1.42$ . ( $L$  is the linear system size, the overbar denotes the spatial average over  $i$ , and the angular brackets stands for the average over configurations of the disorder.) The best scaling of the width,  $w^2 \sim t^{2\beta}$ , is achieved at  $F = F_c \simeq 1.4135$ , with  $\beta = 0.88 \pm 0.03$ , which is shown in Fig. 10. The average position  $H(t)$  increases with an effective exponent which is only slightly lower,  $\beta_H \simeq 0.85$ .

A possibility to determine both,  $\beta$  and the roughness exponent  $\zeta$  is to consider the height-height correlation function  $C(r, t) = \langle [z_{i+r}(t) - z_i(t)]^2 \rangle$ . In the transient regime it scales as

$$C(r, t) \sim r^{2\zeta} \Psi(rt^{-1/z}), \quad (63)$$

where  $\Psi(y)$  is a scaling function. Thus, the exponents  $\zeta$  and  $\beta$  can be obtained by a scaling plot of  $C(r, t)$  which is shown in Fig. 11. The best data collapse at  $F = F_c$  is achieved with  $\zeta(D=1) = z\beta = 1.25 \pm 0.05$  and  $\beta(D=1) = 0.88 \pm 0.03$ .

## B. Simulation of the automaton model

Since the simulations of the continuum equation (62) are computationally expensive, we also study a lattice model [10] of probabilistic cellular automata, which allows to determine effectively the critical exponents in higher dimensions as well.

The automaton model is defined on a  $D + 1$  dimensional hypercubic lattice where each cell  $[i, z]$  (with  $1 \leq i \leq L^D$ ) is assigned a random force  $\eta_{i,z}$  which takes the value 1 with probability  $p$  and  $\eta_{i,z} = -1$  with probability  $1 - p$ . During the motion for a given time  $t$  the local force

$$f_i(t) = \sum_{\langle j \rangle} [z_j(t) - z_i(t)] + m\eta_{i,z_i} \quad (64)$$

is determined for all  $i$ , where the sum is over nearest neighbors  $\langle j \rangle$  only and  $m$  is an integer parameter. The interface configuration is then updated simultaneously for all  $i$ :

$$\begin{aligned} z_i(t+1) &= z_i(t) + 1 & \text{if } v_i > 0 \\ z_i(t+1) &= z_i(t) & \text{otherwise.} \end{aligned} \quad (65)$$

The parameter  $m$  measures the strength of the random force compared to the elastic force and the difference  $p - (1 - p) = 2p - 1$  determines the driving force. The growth rule specified by Eqs. (64) and (65) can be derived from the continuum equation (3) by discretizing the transverse directions  $\mathbf{x}$ , as well as time and the position of the interface  $z(\mathbf{x}, t)$ . In addition, a simple two-state random force  $\eta_{i,z} = \pm 1$  is used which contributes to the computational advantage that one has to handle with integer variables only.

The exponents  $\zeta$  and  $\beta$  are obtained in the same way as in Sec. V.A [10]. In addition, the static roughness exponent  $\zeta$  is determined by measuring the interface width of pinned interfaces for various system sizes  $L$ . The scaling  $w^2 \sim L^{2\zeta}$  at threshold  $p = p_c$  is shown in Fig. 12 ( $D=1,2$  and 3). In  $D=1$  we obtain the same results for  $\zeta$  and  $\beta$  as for Eq. (62)

but with smaller error bars. This supports the expectation that the continuum equation (3) and the automaton model belong to the same universality class.

The results for  $\zeta$  and  $\beta$  are shown in Table 1, together with the other critical exponents  $z \equiv \zeta/\beta$ ,  $\theta$ , and  $\nu$ . The correlation length exponent  $\nu$  is calculated from the scaling relation (60) which was shown to be exact [9]. (Details can be found in Refs. [10] and [11]). The velocity exponent  $\theta$  is determined from the data of Fig. 13 (see Table 1).

### C. Self-organized automaton model (SOAM)

The difficulty of the simulations of Eq. (62) and of the automaton model that the critical region is narrow can be circumvented by “self-organizing” the automaton model (64), (65). Then, the system is always at threshold without tuning a parameter [29]. This can be achieved by using an idea of Havlin et al. [32] and Sneppen [33]: Instead of updating the whole interface configuration simultaneously as in Eq. (65) one increments only that column  $j$  where the local force (64) takes the maximum  $f_{\max} \equiv \max_i[f_i]$  among all  $f_i$  [11],

$$\begin{aligned} z_i(t+1) &= z_i(t) + 1 && \text{if } f_i = f_{\max} \\ z_i(t+1) &= z_i(t) && \text{otherwise.} \end{aligned} \tag{66}$$

To avoid ambiguities, the random forces  $\eta_{i,z}$  are now chosen as real numbers in the interval  $0 \leq \eta < 1$ . A very similar model has been independently introduced by Roux and Hansen [34].

We determine the roughness exponent  $\zeta$  of the SOAM by simulating interfaces according to the rules (64), (66) and measure the width during a sufficiently long time interval for different system sizes. The results [11]  $\zeta(D=1) = 1.24 \pm 0.01$ ,  $\zeta(D=2) = 0.75 \pm 0.01$ , and  $\zeta(D=3) = 0.34 \pm 0.01$  are consistent with the results of the automaton model.

### D. Comparison with analytical results

We now compare the numerical results with the analytical exponents which are obtained by an extrapolation of the results (61) of the  $\epsilon$ -expansion (see Table 1). It should be emphasized that the equation of motion (3) is not a useful description of an interface in a two-dimensional medium ( $D=1$ ) because higher gradient terms are relevant. This is in agreement with the unphysical result  $\zeta(D=1) \simeq 1.25 > 1$ . Nonetheless, the considered interfaces are stable and self-affine because Eq. (3) and the automaton models (64), (65), and (66) do not allow overhangs. We include the case  $D=1$  in Table 1 in order to compare the analytical and numerical results for Eq. (3).

The simulations support the analytical results: In  $D=3$  ( $\epsilon=1$ ) the analytical results deviate from the numerical values by only a few percent. In agreement with the expectation of an  $\epsilon$ -expansion in  $D=4-\epsilon$  the deviations become larger with decreasing  $D$ . The numerical results in Table 1 are consistent with the exact scaling relation (11). However, the results for the roughness exponents are clearly inconsistent with the suggestion [9] that  $\zeta = (4-D)/3$  is exact. Assuming that there are no higher-order corrections to  $\zeta$  [9], the

numerical results indicate that there are non-perturbative corrections to  $\zeta$ , a possibility mentioned by Narayan and Fisher [9].

The exactness of the result  $\zeta = (4 - D)/3$  would have meant that an interface at equilibrium ( $F = 0$ ,  $T > 0$ ) and a driven interface at threshold  $F_c$  have the same roughness exponent although the underlying physics is different. The simulations show that the driven interface is rougher than the interface in equilibrium.

The Harris condition (13) for a sharp depinning transition is fulfilled as an inequality by the numerical values.

## VI. SUMMARY

In this paper we investigated the behavior of an elastic interface, which is driven by a homogeneous force  $F$  through a medium with short-range correlated random forces. It was made plausible that this problem can be described by the equation of motion (3) for a planar interface. It was found that  $D_c = 4$  is the upper critical dimension. For  $D > D_c$  and weak disorder, the interface is always smooth and there is no threshold for driven motion if the random force varies sufficiently slowly in space. However, we showed by considering a mean field theory that, a nonvanishing threshold  $F_c > 0$  can be produced by a random force with a cusp singularity ( $\Delta'(0^+) < 0$ ) of its correlator  $\Delta(z)$ . Below  $D_c$  the interface becomes rough above the Larkin length  $L_c$ . The correlation length  $\xi$  is a second important length scale, which diverges when approaching the critical point  $F_c$ . The results of the perturbation theory diverge with a power of  $\xi$ .

A simple three-parameter RG is not a way out of these divergences, because the second moment  $Q_2 = \Delta''(0)$  of the correlator and therefore the inverse mobility  $\lambda$  diverge under renormalization at  $L = L_c$ . Extending the space of renormalizable parameters to all moments  $Q_{2n} = \Delta^{(2n)}(0)$  of the correlator, i.e. to the whole *function*  $\Delta(z)$ , we found that the above divergences correspond to a cusp singularity of  $\Delta(z)$  at the origin. With the interpretation  $Q_{2n} = \Delta^{(2n)}(0^+)$  a consistent RG scheme could be constructed. The cusp singularity  $\Delta'(0^+) < 0$  produces a finite threshold  $F_c$ , similar to the mean field theory [23]. Above the threshold, the RG is stopped at the correlation length  $L = \xi$ , above which one crosses over to a EW regime, where the random forces act independently on the moving interface. The behavior of the interface at different length scales  $L$  and driving forces  $F$  can be summarized in a phase diagram (see Fig. 9).

The exponents in the critical regime  $L_c < L < \xi$  were calculated to first order in  $\epsilon = 4 - D$  (see Eq. (61)). Although the result for the roughness exponent  $\zeta \simeq \epsilon/3$  coincides with that of the equilibrium problem to first order in  $\epsilon$ , our numerical simulations show that the roughness at the threshold and zero temperature is larger than that in equilibrium ( $F = 0, T > 0$ ). As expected, the velocity exponent  $\theta$  decreases when the dimension is decreased, i.e. for a rougher interface the onset of the motion at  $F_c$  is more abrupt. Our results for the correlation length exponent  $\nu$  fulfill a Harris-like criterion to observe a sharp transition as an equality for the first-order results and as an inequality for the numerical results.

## ACKNOWLEDGEMENTS

The research is partially supported by the Deutsche Forschungsgemeinschaft through Sonderforschungsbereich 166 and 341.

## APPENDIX A: VELOCITY

In this Appendix the perturbative calculation of the velocity  $v$  of the interface is discussed. We give two examples how typical integrals for the corrections to the velocity can be calculated.

### 1. First-order correction

The velocity  $v$  can be obtained by iterating Eq. (22): The  $n$ -th order iteration for  $\tilde{h}(\mathbf{k}, w)$  follows from (22) by using the  $(n-1)$ -th order iteration on its *rhs*. (The zeroth order iteration of  $\tilde{h}$  vanishes.) After truncating this procedure at the order which is needed, the resulting equation is averaged over the disorder, which gives on the *lhs*  $\langle \tilde{h}(\mathbf{k}, \omega) \rangle = 0$ , while the *rhs* is a function of  $v$ . For example, the lowest-order correction (Fig. 4) to  $v_0 = F/\lambda$  is obtained from the second-order iteration

$$\frac{F - \lambda v}{\lambda v} \simeq -\frac{1}{\lambda v} \int_q \int_{\mathbf{p}} \frac{i q \Delta_q \tilde{\Delta}_{\parallel}(\mathbf{p})}{\gamma \mathbf{p}^2 - i \lambda v q} \equiv I_1, \quad (\text{A1})$$

where we have included the Fourier transform  $\tilde{\Delta}_{\parallel}(\mathbf{p})$  of the correlator along the interface (see Eq. (25)).

First, we make  $I_1$  real, perform the angular integration and take the correlator  $\tilde{\Delta}_{\parallel}(\mathbf{p})$  into account by truncating the  $p$ -integration at  $1/a_{\parallel}$ :

$$I_1 \simeq K_D \int_q q^2 \Delta_q \int^{1/a_{\parallel}} dp \frac{p^{D-1}}{\gamma^2 p^4 + (\lambda v q)^2}, \quad (\text{A2})$$

where  $K_D^{-1} = 2^{D-1} \pi^{D/2} \Gamma(D/2)$ . For  $D > 4$  this integral converges for all  $v$  as long as  $a_{\parallel}$  is finite. For  $D < 4$ , however, the limit  $v \rightarrow 0$  causes a divergence at small  $p$ . If we set  $a_{\parallel} = 0$ , the integral (A2) diverges at large  $p$  when  $4 - D = \epsilon \rightarrow 0$ .

After introducing the new variable  $y = p/\sqrt{\lambda v q/\gamma}$ , we get

$$I_1 \simeq \frac{K_D}{\gamma^{D/2}} (\lambda v)^{-\epsilon/2} \int_q q^{D/2} \Delta_q \int^{\sqrt{\gamma/\lambda v q/a_{\parallel}}} dy \frac{y^{D-1}}{y^4 + 1}. \quad (\text{A3})$$

The divergence with  $v \rightarrow 0$  is now outside the integral and we can set the upper limit to infinity and thereby getting the desired leading term proportional to  $1/\epsilon$ :

$$I_1 \simeq -\frac{K_D}{\gamma^2} \xi_0^{\epsilon} \Delta''(0) \int_1^{\infty} dy y^{D-5}, \quad (\text{A4})$$

where Eq. (26) was used. Hence one gets the result

$$\frac{F - \lambda v}{\lambda v} \simeq cQ_2 \frac{1}{\epsilon} \xi_0^\epsilon \equiv \delta\lambda^{(1)}/\lambda, \quad (\text{A5})$$

which is the same as Eq. (37).

However, for very large  $v$ ,  $\xi_0 \ll a_{\parallel}$ , i.e.  $\sqrt{\lambda v q / \gamma}$  can no longer be regarded as a lower cutoff for the  $p$ -integration. The latter has to be truncated at an upper cutoff  $1/a_{\parallel}$ . In this case one can introduce the new variable  $q' = \lambda v q / \gamma p^2$ . Then the integrals in Eq. (A2) can be carried out:

$$\frac{F - \lambda v}{\lambda v} \simeq \frac{K_D}{\lambda^2 v^2} \frac{a_{\parallel}^{-D}}{D} \int_{q'} \Delta_{q'} \frac{q'^2}{1 + q'^2} \simeq \Delta(0) \frac{K_D}{\lambda^2 v^2} \frac{a_{\parallel}^{-D}}{D}. \quad (\text{A6})$$

As expected, the correction to  $F - \lambda v$  vanishes for large  $v$ , where Eq. (3) is of EW-type.

## 2. Second-order correction

Next we extend the calculation of the velocity to second order. To this end Eq. (22) is iterated as described above. The second order diagrams for the velocity are shown in Fig. 14. Since we want to use the perturbation theory to construct a renormalization group expansion in  $D = 4 - \epsilon$  we only calculate the leading order terms in  $\epsilon$ . The expression for diagram 14a) is given by

$$I_2 \equiv \int_q \int_{q'} \int_{\mathbf{p}} \int_{\mathbf{p}'} \Delta_q \Delta_{q'} \tilde{\Delta}_{\parallel}(\mathbf{p}) \tilde{\Delta}_{\parallel}(\mathbf{p}') i^3 q^2 q' \\ \times \frac{1}{\gamma \mathbf{p}^2 + i\lambda v q} \frac{1}{\gamma \mathbf{p}'^2 + i\lambda v q'} \frac{1}{\gamma(\mathbf{p} + \mathbf{p}')^2 + i\lambda v(q + q')}. \quad (\text{A7})$$

The integrals will be evaluated below. The result is

$$\lambda v \frac{1}{2} \left( \frac{\delta\lambda^{(1)}}{\lambda} \right). \quad (\text{A8})$$

The calculation of diagram 14b) is very similar and gives the same contribution as (A8). Diagrams 14c) and 14d) correspond to a renormalization of the response function and also contribute the term (A8). The sum of the diagrams 14e)-g) is equal to zero, diagram 14h) cancels with 14j) and diagram 14i) cancels with 14k). If we collect all diagrams up to second order we finally obtain

$$\lambda_{eff} = \lambda \left[ 1 + \frac{\delta\lambda^{(1)}}{\lambda} + 2 \left( \frac{\delta\lambda^{(1)}}{\lambda} \right)^2 + \dots \right]. \quad (\text{A9})$$

As an example for the evaluation of second-order diagrams we calculate the contribution (A7) of diagram 14a). The integrals over  $q$  and  $q'$  do not vanish only if the powers of  $q$  and  $q'$  are even. Thus  $I_2$  is

$$I_2 = \int_q \int_{q'} \int_{\mathbf{p}} \int_{\mathbf{p}'} \Delta_q \Delta_{q'} \tilde{\Delta}_{\parallel}(\mathbf{p}) \tilde{\Delta}_{\parallel}(\mathbf{p}') q^2 q'^2 v$$

$$\times \frac{\mathbf{p}^2 \mathbf{p}'^2 + \mathbf{p}^2 (\mathbf{p} + \mathbf{p}')^2}{[\gamma^2 \mathbf{p}^4 + (\lambda v q)^2] [\gamma^2 \mathbf{p}'^4 + (\lambda v q')^2]} \frac{1}{[\gamma^2 (\mathbf{p} + \mathbf{p}')^4 + (\lambda v (q + q'))^2]} \quad (\text{A10})$$

$$\equiv \int_q \int_{q'} \Delta_q \Delta_{q'} q^2 q'^2 v I_k. \quad (\text{A11})$$

We consider here only the first term with  $\mathbf{p}^2 \mathbf{p}'^2$  in Eq. (A10) because the second one cancels with a term of the diagram in Fig. 14b). We have seen that the integration over  $p$  gives the important leading divergences, while the  $q$ -integration does not yield divergent factors. Thus, for simplicity we set in Eq. (A11)  $q = q'$ , and introduce new variables  $\mathbf{y} = \mathbf{p}/\sqrt{\lambda v q/\gamma}$ , and  $\mathbf{y}' = \mathbf{p}'/\sqrt{\lambda v q/\gamma}$  and treat the limits as in the calculation of the first order correction. Then we obtain

$$I_k \simeq \int_1^{\sqrt{\gamma/\lambda v q/a_{\parallel}}} \frac{d^D y}{(2\pi)^D} \int_1^{\sqrt{\gamma/\lambda v q/a_{\parallel}}} \frac{d^D y'}{(2\pi)^D} \frac{1}{\mathbf{y}^2} \frac{1}{\mathbf{y}'^2} \frac{1}{(\mathbf{y} + \mathbf{y}')^4}, \quad (\text{A12})$$

where the range of integration refers to the absolute values of  $\mathbf{y}$  and  $\mathbf{y}'$ . Again, the important divergence is at large  $y$  and  $y'$ , so that we can introduce a smooth cutoff for small  $y$  and  $y'$  and first perform the  $y'$ -integration and set the upper limit to infinity:

$$I_k \simeq \int_{\mathbf{y}} \frac{1}{(\mathbf{y}^2 + 1)} I'_k$$

with

$$I'_k = \int_{\mathbf{y}'} \frac{1}{(\mathbf{y}'^2 + 1)} \frac{1}{[(\mathbf{y} + \mathbf{y}')^2 + 1]^2}. \quad (\text{A13})$$

This  $D$ -dimensional integral can be evaluated by introducing a Feynman-parameter  $x$  [36]

$$I'_k = \int_{\mathbf{y}'} \Gamma(3) \int_0^1 dx x \left\{ (1-x)(\mathbf{y}'^2 + 1) + x[(\mathbf{y} + \mathbf{y}')^2 + 1] \right\}^{-3}. \quad (\text{A14})$$

Using the general formula

$$\int_{\mathbf{y}} [\mathbf{y}^2 + 2\mathbf{y}\mathbf{y}' + m^2]^{-\alpha} = \frac{K_D}{2} \frac{\Gamma\left(\frac{D}{2}\right) \Gamma\left(\alpha - \frac{D}{2}\right)}{\Gamma(\alpha)} [m^2 - \mathbf{y}'^2]^{(D/2)-\alpha}, \quad (\text{A15})$$

one obtains

$$I'_k = \frac{K_D}{2} \Gamma(D/2) \Gamma(3 - D/2) \int_0^1 dx x \left\{ \mathbf{y}^2 (x - x^2) + 1 \right\}^{(D/2)-3}. \quad (\text{A16})$$

The  $y$ -integration is also performed by introducing a Feynman-parameter  $x'$ .

$$I_k \simeq \left( \frac{K_D}{2} \right)^2 \Gamma^2(D/2) \Gamma(\epsilon) \times \int_0^1 dx \int_0^1 dx' x x'^{\epsilon/2} \{ x' [x(1-x) - 1] + 1 \}^{(\epsilon/2)-2}. \quad (\text{A17})$$



With  $\epsilon/2 = \epsilon' \rightarrow 0$  this integral is logarithmically divergent. The prefactor of this logarithmic divergence is the same as the prefactor of the  $1/\epsilon$  term for small  $\epsilon$ . Thus, we consider only the integral Eq. (A17) for  $\epsilon' = \epsilon/2 = 0$  and calculate the desired prefactor. The integrals are then elementary and the prefactor is calculated to one. Then we obtain with  $\Gamma(2\epsilon') \simeq 1/(2\epsilon')$

$$I_k \simeq K_D^2 \frac{1}{2} \frac{1}{\epsilon^2}. \quad (\text{A18})$$

With Eq. (A11) the result (A8) follows.

## APPENDIX B: VERTEX CORRECTION

In this Appendix we outline the calculation which leads to the renormalization of moments resulting in Eq. (46). The diagrammatic representation of the bare moments  $Q_{2n}$  is shown in Fig. 7a), where all incoming and outgoing momenta conjugated to  $\mathbf{x}$  are set to zero. According to Eq. (45) the analytical expression associated with the diagram a) is exactly  $Q_{2n}$ . The diagrams contributing to the renormalization of the moments up to the one-loop order are shown in Fig. 7b)-d). In each of these diagrams, one has only one integration over the internal momentum conjugated to the space argument of the interface height  $h(\mathbf{x})$ . This integration has the form  $\int_{\mathbf{p}} G_0^2(\mathbf{p})$  and yields for all diagrams under consideration the same factor  $c\xi_0^\epsilon/\epsilon$ . Additionally to this integration there is also an integration over the momenta  $q_1$  and  $q_2$  conjugated to the argument of the disorder correlator  $\Delta(z)$ . The momenta  $q_1$  and  $q_2$  are associated with the dotted lines in one-loop diagrams in Fig. 7.

Let us consider the diagram b). The number of arrows starting at crossing points of dotted lines with the continuous line is  $n$  for both upper and the down continuous lines. The distribution of arrows between the both crossing point along a continuous line is arbitrary. The sum of the arrows should obey the condition  $n_1 + n_2 = n$ . According to Eq. (22) the factor  $(\pm iq)^m$  is associated with each crossing point with  $m$  being the number of lines starting at the point under consideration. The sign  $+$  has to be taken if the dotted line belonging to the crossing point goes out from the point,  $-$  if the dotted line goes into the crossing point. In the following we designate  $-q$  by  $\tilde{q}$ . Summing over all possible distributions of arrows between the two crossing points of the top line in the diagram b) we get the factor

$$i^{n+1} q_1 (q_1 + \tilde{q}_2)^n. \quad (\text{B1})$$

The factor associated with the distribution of arrows on the down line in b) is

$$i^{n+1} \tilde{q}_1 (\tilde{q}_1 + q_2)^n, \quad (\text{B2})$$

so that the factor associated with the whole diagram b) is

$$(-1)^{n+1} q_1 \tilde{q}_1 (q_1 + \tilde{q}_2)^n (\tilde{q}_1 + q_2)^n. \quad (\text{B3})$$

Analogously the factor associated with the diagram c) is given by

$$(-1)^{n+1} q_1 q_2 (q_1 + \tilde{q}_2)^n (\tilde{q}_1 + q_2)^n. \quad (\text{B4})$$

The factor associated with b) and c) is the sum of (B3) and (B4)

$$(q_1 + \tilde{q}_2)^{2n+1} q_1 = \sum_{k=1}^{2n+1} C_k^{2n+1} q_1^{2n+2-k} \tilde{q}_2^k + q_1^{2n+2} q_2^0, \quad (\text{B5})$$

where  $C_i^j = \binom{j}{i}$  are the binomial coefficients. The diagram d) in Fig. 7 gives the factor

$$- q_1^{2n+2} q_2^0, \quad (\text{B6})$$

which compensates the last term in Eq. (B5). Thus, the part of the diagrams b) - d) depending on  $q_1$  and  $q_2$  is given by

$$\sum_{k=1}^{2n+1} C_k^{2n+1} q_1^{2n+2-k} \tilde{q}_2^k. \quad (\text{B7})$$

To obtain the analytical expression associated with b)-d) we have to multiply (B7) with  $\Delta(q_1)\Delta(q_2)$  and integrate over  $q_1$  and  $q_2$ . Taking into account that only the even moments of the disorder correlator  $\Delta(z)$  are non zero we get from (B7)

$$\sum_{k=1}^n C_{2k}^{2n+1} Q_{2k} Q_{2n-2k+2}. \quad (\text{B8})$$

The whole correction of b)-d) is obtained from (B8) by multiplying the latter with the factor  $c\xi_0^\epsilon/\epsilon$ . Finally, the contribution from the diagrams a)-d) in Fig. 7 is

$$Q_{2n} + \sum_{k=1}^n C_{2k}^{2n+1} Q_{2k} Q_{2n-2k+2} c\xi_0^\epsilon/\epsilon. \quad (\text{B9})$$

The latter gives the renormalization of the moments of the disorder correlator up to the one-loop order.

### APPENDIX C: FUNCTIONAL FLOW EQUATION

In this Appendix it is shown how the vertex corrections of the moments  $Q_{2n}$  in Eq. (46) can be put together in a functional flow equation for  $\Delta(z)$ .

The flow equation can be formally obtained by differentiating Eq. (26)

$$\frac{\partial \Delta(z)}{\partial \ln L} = \sum_{n=0}^{\infty} \frac{(iz)^{2n}}{(2n)!} L \frac{\partial Q_{2n}}{\partial L}, \quad (\text{C1})$$

where  $Q_{2n}$  is identified with the effective moments  $Q_{2n,eff}$  which depend on the upper cutoff  $L = \xi_0$ . Differentiating Eq. (46) and writing  $Q_{2n,eff} = Q_{2n}$  one gets

$$L \frac{\partial Q_{2n}}{\partial L} = cL^\epsilon \sum_{j=1}^n C_{2j}^{2n+1} Q_{2j} Q_{2(n-j+1)}. \quad (\text{C2})$$

To construct a functional flow equation the *rhs* of Eq. (C1) has to be expressed as a function of  $\Delta(z)$ . To this end one first extends the summation over  $j$  to  $0 \leq j \leq n$  and

subtracts the term with  $j = 0$  separately. Introducing the new index  $k = n - j$  and using  $C_{2j}^{2n+1} = C_{2(n-j)+1}^{2n+1}$ , the *rhs* of Eq. (C1) can be written as

$$\sum_{n=0}^{\infty} \frac{(iz)^{2n}}{(2n)!} \sum_{j=0}^n C_{2j+1}^{2n+1} Q_{2j+2} Q_{2n-2j} - Q_0 \sum_{n=0}^{\infty} \frac{(iz)^{2n}}{(2n)!} Q_{2n+2}, \quad (\text{C3})$$

where  $j$  is written for  $k$  and the factor  $cL^\epsilon$  is skipped. With Eq. (26) the second term can be expressed as

$$- \frac{\partial^2}{\partial(iz)^2} \Delta(z) \Delta(0). \quad (\text{C4})$$

The first term in (C3) can be written as

$$\frac{\partial}{\partial(iz)} \left\{ \frac{\partial}{\partial(iz')} \sum_{n=0}^{\infty} \sum_{j=0}^n \frac{(iz')^{2j+2}}{(2j+2)!} Q_{2j+2} \right\}_{z'=z} \frac{(iz)^{2n-2j}}{(2n-2j)!} Q_{2n-2j} \Bigg\}. \quad (\text{C5})$$

Writing down the sums over  $n$  and  $j$  term by term, one easily sees that (C5) is equal to

$$\frac{\partial}{\partial(iz)} \left\{ \frac{\partial}{\partial(iz')} \sum_{j=1}^{\infty} \frac{(iz')^{2j}}{(2j)!} Q_{2j} \right\}_{z'=z} \sum_{n=0}^{\infty} \frac{(iz)^{2n}}{(2n)!} Q_{2n} \Bigg\}. \quad (\text{C6})$$

The range of the summation over  $j$  can be extended to the vanishing term  $j = 0$ . Using Eq. (26), (C6) can be identified with

$$\frac{\partial}{\partial(iz)} \left\{ \frac{\partial}{\partial(iz')} \Delta(z') \right\}_{z'=z} \Delta(z) \Bigg\} = -\frac{1}{2} \frac{\partial^2}{\partial z^2} \Delta^2(z). \quad (\text{C7})$$

Now we can put the first and second term of Eq. (C3) together and insert it in Eq. (C1):

$$\frac{\partial}{\partial \ln L} \Delta(z) = -cL^\epsilon \frac{d^2}{dz^2} \left[ \frac{1}{2} \Delta^2(z) - \Delta(z) \Delta(0) \right], \quad (\text{C8})$$

which is the functional flow equation (50).

## REFERENCES

- [1] For reviews see, e.g., T. Nattermann, P. Rujan, Int. J. Mod. Phys. B **3** (1989) 1597; D. P. Belanger, A. P. Young, J. Magn. Magn. Mat. **100** (1991) 272; G. Forgacs, R. Lipowsky, Th. M. Nieuwenhuizen, in Phase transitions and critical phenomena, Vol. 14, edited by C. Domb, J. L. Lebowitz, Academic Press, London 1991
- [2] K. B. Efetov, A. I. Larkin, Sov. Phys. JETP **45** (1977) 1236
- [3] H. Fukuyama, P. A. Lee, Phys. Rev. B **17** (1978) 535; P. A. Lee, T. M. Rice, Phys. Rev. B **19** (1979) 3970
- [4] D. S. Fisher, Phys. Rev. Lett. **50** (1983) 1486; Phys. Rev. B **31** (1985) 1396
- [5] O. Narayan, D. S. Fisher, Phys. Rev. Lett. **68** (1992) 3615; Phys. Rev. B **46** (1992) 11520
- [6] A. I. Larkin, Yu. N. Ovchinnikov, Sov. Phys. JETP **38** (1974) 854; J. Low Temp. Phys. **34** (1979) 409
- [7] A. I. Larkin, Sov. Phys. JETP **31** (1970) 784
- [8] T. Nattermann, S. Stepanow, L.-H. Tang, H. Leschhorn, J. Phys. II France **2** (1992) 1483
- [9] O. Narayan, D. S. Fisher, Phys. Rev. B, **48** (1993) 7030
- [10] H. Leschhorn, Physica A **195** (1993) 324
- [11] H. Leschhorn, Ph.D. thesis, Ruhr-Universität Bochum 1994
- [12] S. A. Allen, J. W. Cahn, Acta Metall. **27** (1979) 1085
- [13] R. Bausch, V. Dohm, H. K. Janssen, R. K. P. Zia, Phys. Rev. Lett. **47** (1981) 1837
- [14] M. Kardar, G. Parisi, Y.-C. Zhang, Phys. Rev. Lett. **56**, (1986) 889; for a review see, e.g., J. Krug, H. Spohn, Solids Far From Equilibrium: Growth, Morphology, and Defects, edited by C. Godrèche, Cambridge University Press, Cambridge 1990
- [15] M. V. Feigel'man, Sov. Phys. JETP **58** (1983) 1076
- [16] R. Bruinsma, G. Aeppli, Phys. Rev. Lett. **52** (1984) 1547
- [17] J. Koplik, H. Levine, Phys. Rev. B **32** (1985) 280; D. A. Kessler, H. Levine, Y. Tu, Phys. Rev. A **43** (1991) 4551
- [18] A. A. Middleton, Phys. Rev. Lett. **68** (1992) 670
- [19] S. F. Edwards, D. R. Wilkinson, Proc. R. Soc. London, Ser. A **381** (1982) 17
- [20] A. B. Harris, J. Phys. C **7** (1974) 1671
- [21] H. Leschhorn, J. Phys. A **25** (1992) L555
- [22] L.-H. Tang, S. Stepanow, unpublished
- [23] In contrast to mean field theory, the cusp in the random force correlator need not be put in by hand for  $D < D_c$ . We expect that the cusp singularity occurs spontaneously due to an avalanche-like collective motion.
- [24] P. C. Hohenberg, B. I. Halperin, Rev. Mod. Phys. **49** (1977) 435
- [25] Field-theoretic methods [26] and an expansion around mean field theory [9] do not obtain a correction to  $\gamma$  at all. This discrepancy to Eq. (36) does not influence the critical behavior of the depinning transition.
- [26] S. Stepanow, Ann. Physik **1** (1992) 423
- [27] D. S. Fisher, Phys. Rev. Lett. **56** (1986) 1964
- [28] G. Parisi, Europhys. Lett. **17** (1992) 673

- [29] P. Bak, C. Tang, K. Wiesenfeld, Phys. Rev. Lett. **59** (1987) 381
- [30] Z. Csahók, K. Honda, T. Vicsek, J. Phys. A **26** (1993) L171; Z. Csahók, K. Honda, E. Somfai, M. Vicsek, T. Vicsek, Physica A **200** (1993) 136
- [31] M. Dong, M. C. Marchetti, A. A. Middleton, V. Vinokur, Phys. Rev. Lett. **70** (1993) 662
- [32] S. Havlin, A.-L. Barabási, S. V. Buldyrev, C. K. Peng, M. Schwartz, H. E. Stanley, T. Vicsek, in Growth Patterns in Physical Sciences and Biology, edited by E. Louis, L. Sander, P. Meakin, Plenum, New York 1993
- [33] K. Sneppen, Phys. Rev. Lett. **69** (1992) 3539
- [34] S. Roux, A. Hansen, J. Phys. I France **4** (1994) 515
- [35] N. Martys, M. Cieplak, M. O. Robbins, Phys. Rev. Lett. **66** (1991) 1058; N. Martys, M. O. Robbins, M. Cieplak, Phys. Rev. B **44** (1991) 12294
- [36] see for example D. J. Amit, Field Theory, the Renormalization Group, and Critical Phenomena, McGraw-Hill 1978

## FIGURES

FIG. 1. Interface velocity  $v$  as a function of the driving force  $F$ .

FIG. 2. The random force correlator  $\Delta(z)$  for (a) random-fields, (b) random bonds, and (c) charge-density waves.

FIG. 3. The diagrammatic representation of Eq. (22) (see text).

FIG. 4. First-order correction to the velocity (see Eq. (29)). The average over the quenched randomness is represented by the connection of two outgoing dotted lines, which build up a “loop”.

FIG. 5. The response function  $G(\mathbf{k}, \omega)$ , represented as a double line with an arrow, and its one-loop expansion (see Eq. (33)).

FIG. 6. Lowest-order diagram to the interface width (Eq. (39)).

FIG. 7. Diagrams illustrating the renormalization of the moments of  $\Delta(z)$ . The diagrams shown contribute to the renormalization of  $Q_{2n}$ . In diagram b) and c) the number of outgoing lines have to fulfill the condition  $n_1 + n_2 = n_3 + n_4 = n$ .

FIG. 8. When starting with a smeared delta function (full line in figure on the *lhs*) the second moment  $Q_2 = \Delta''(0)$  is negative. Under the renormalization on scales  $L < L_c$  the curvature at the origin becomes greater and  $\Delta(z)$  becomes more peaked (dotted line). At  $L \simeq L_c$  the curvature diverges and the fixed-point solution has a cusp singularity (figure on the *rhs*).

FIG. 9.  $F - L$  phasediagram (see text).

FIG. 10. Scaling of the average position  $H(t)$  (triangles) and interface width  $w(t)$  (circles) at threshold  $F_c$  from a simulation of Eq. (62) in  $D = 1$ . The system size is  $L = 16384$ ,  $\Delta t = 0.125$ , and the data are averaged over 30 realizations of the disorder.

FIG. 11. Scaling plot of the height-height correlation function  $C(r, t)$  from the same runs as in Fig. 10. The same plotting symbol is used for data at a given time  $t$ .

FIG. 12. The width  $w^2$  of pinned interfaces as a function of the system size  $L$  from simulations of the automaton model for  $D = 1$ ,  $g = 1$ ,  $p = p_c \simeq 0.8004$  (open circles),  $D = 2$ ,  $g = 6$ ,  $p = p_c \simeq 0.74446$  (filled circles), and  $D = 3$ ,  $g = 8$ ,  $p = p_c \simeq 0.63165$  (squares).

FIG. 13. Interface velocity  $v$  as a function of the driving force  $p - p_c$  for  $D = 1$ ,  $g = 1$ ,  $L \leq 262144$  (open circles),  $D = 2$ ,  $g = 6$ ,  $L^2 = 1024^2$  (filled circles), and  $D = 3$ ,  $g = 8$ ,  $L \leq 110^3$  (squares).

FIG. 14. Second-order corrections to the velocity.

# TABLES

Exponent	$D$	analytical	numerical
velocity $\theta$	1	1/3	$0.25 \pm 0.03$
	2	2/3	$0.64 \pm 0.02$
	3	0.866..	$0.84 \pm 0.02$
roughness $\zeta$	1	1	$1.25 \pm 0.01$
	2	2/3	$0.75 \pm 0.02$
	3	1/3	$0.35 \pm 0.01$
roughening $\beta$	1	3/4	$0.88 \pm 0.02$
	2	0.4286..	$0.48 \pm 0.01$
	3	0.1875	$0.20 \pm 0.01$
dynamical $z = \zeta/\beta$	1	4/3	$1.42 \pm 0.04$
	2	1.555..	$1.56 \pm 0.06$
	3	1.777..	$1.75 \pm 0.15$
correlation length $\nu$ $\nu = 1/(2 - \zeta)$	1	1	$1.33 \pm 0.02$
	2	3/4	$0.80 \pm 0.01$
	3	3/5	$0.606 \pm 0.004$

TABLE I. Analytical and numerical results for the critical exponents for interface dimensions  $D = 1, 2$  and  $3$ . The analytical values are obtained by an extrapolation of the results (61) of the  $\epsilon$ -expansion.



Figure 1

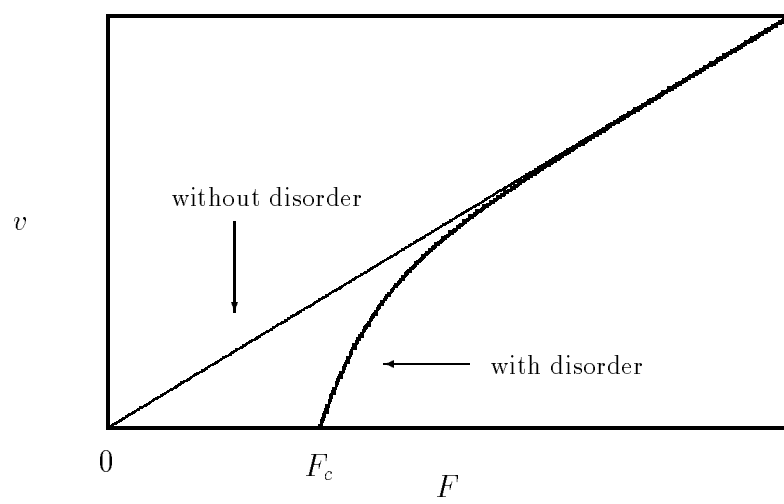


Figure 2

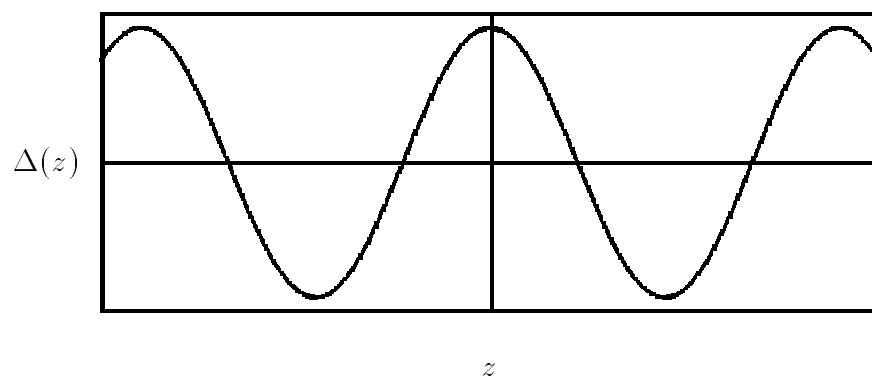
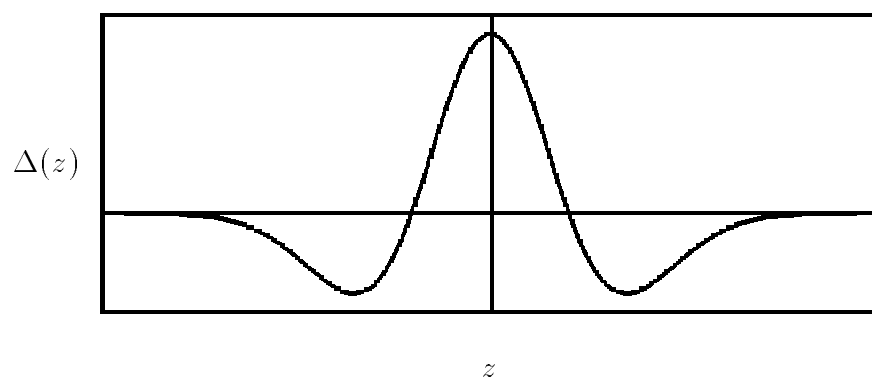
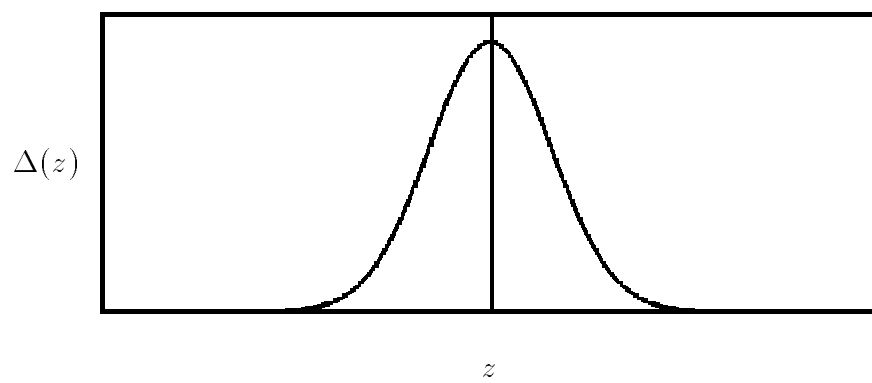


Figure 3

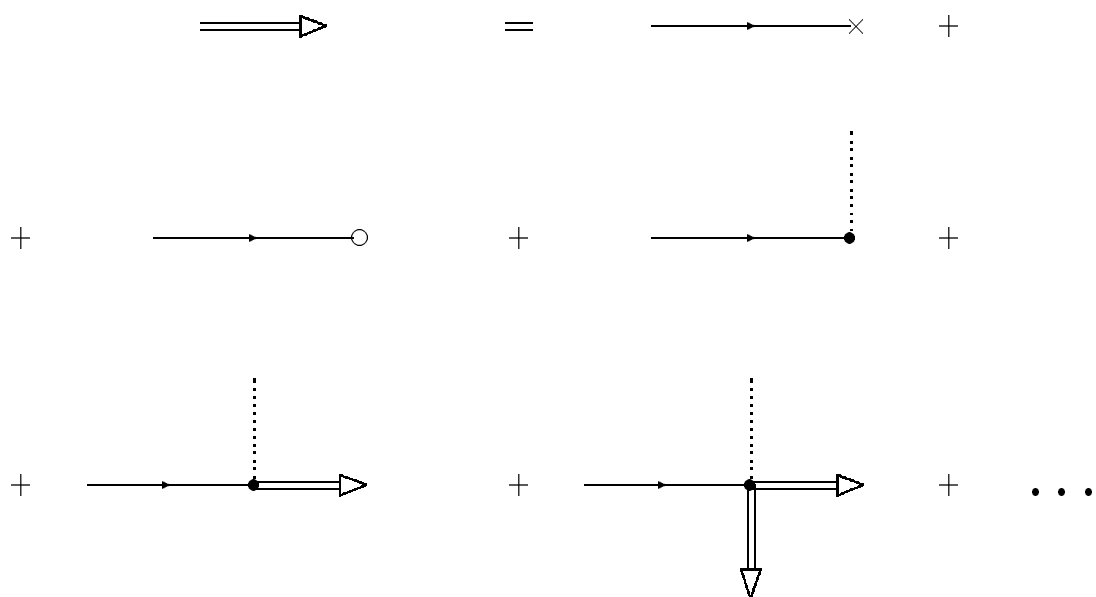


Figure 4

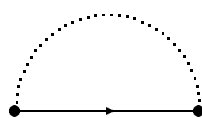


Figure 5

$$\begin{array}{c}
 \text{Diagram 1} \\
 \text{Diagram 2}
 \end{array}
 =
 \begin{array}{c}
 \text{Diagram 3} \\
 \text{Diagram 4}
 \end{array}
 + \dots$$

Figure 5 illustrates a diagrammatic equation. On the left, two diagrams are shown stacked vertically. The top diagram consists of two parallel horizontal lines with a small triangle pointing to the right between them. The bottom diagram shows a horizontal line with an arrow pointing right, a vertical line segment with an arrow pointing up, and a dotted semi-circular arc connecting the top of the vertical line back to the horizontal line. To the right of these is an equals sign, followed by two more diagrams stacked vertically. The top diagram is a single horizontal line with an arrow pointing right. The bottom diagram is a horizontal line with an arrow pointing right, two dots on it, and a dotted semi-circular arc connecting the two dots. To the right of these is a plus sign, followed by an ellipsis (...).

Figure 6

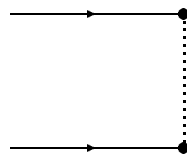


Figure 7

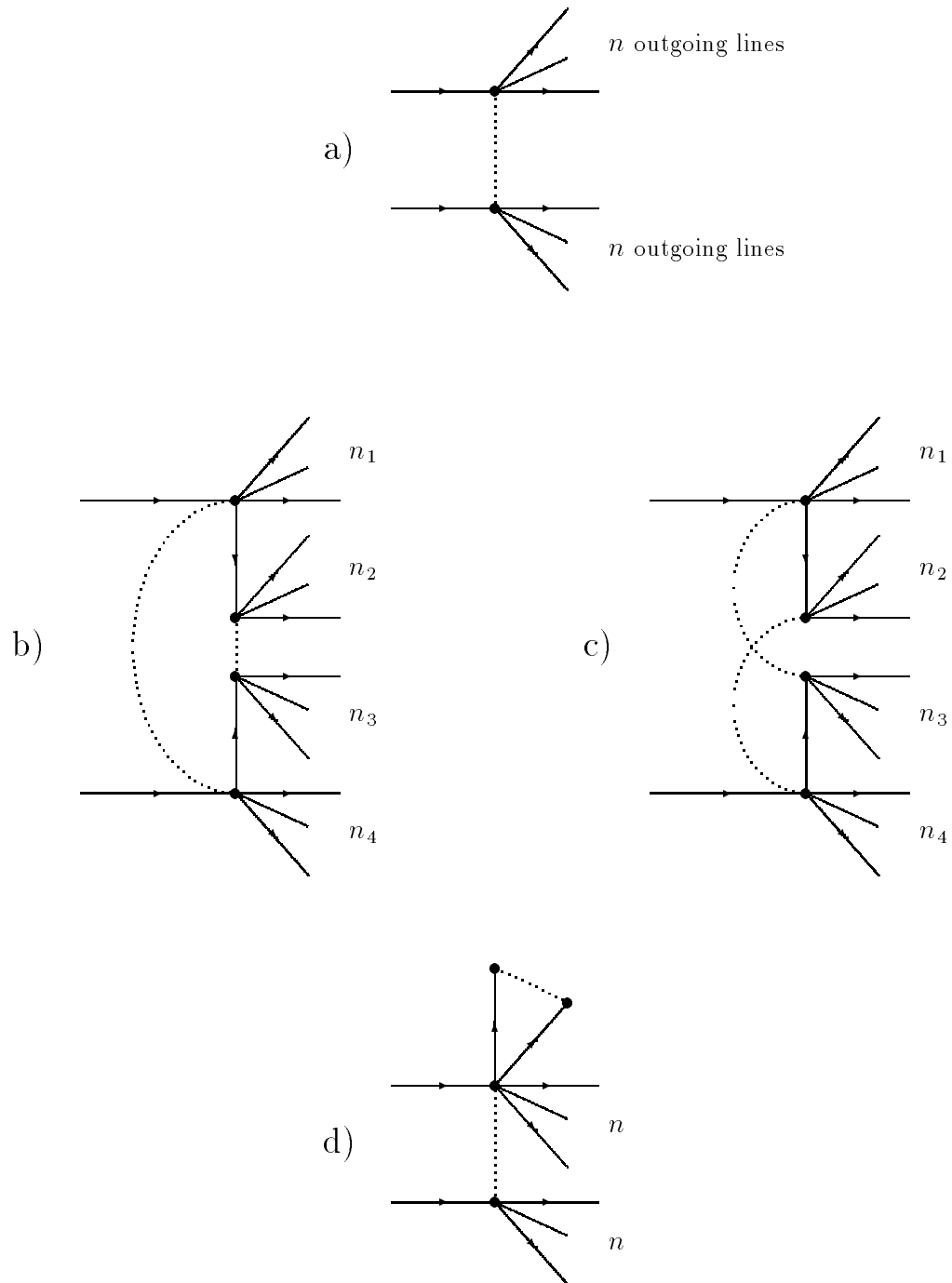


Figure 8

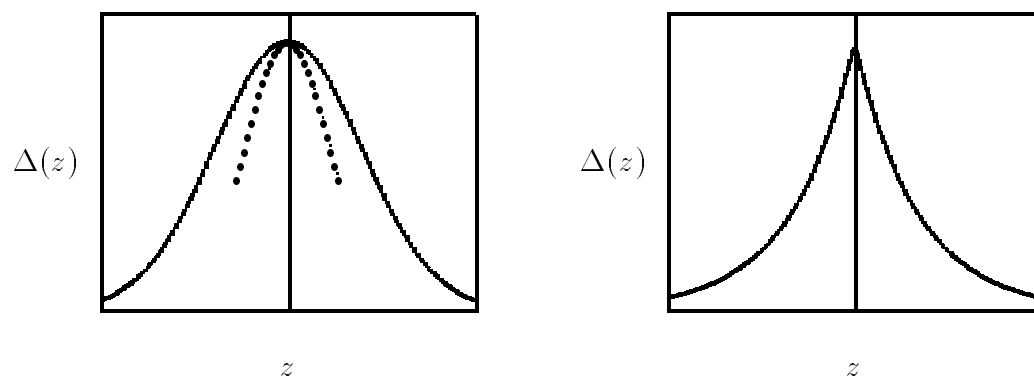


Figure 9

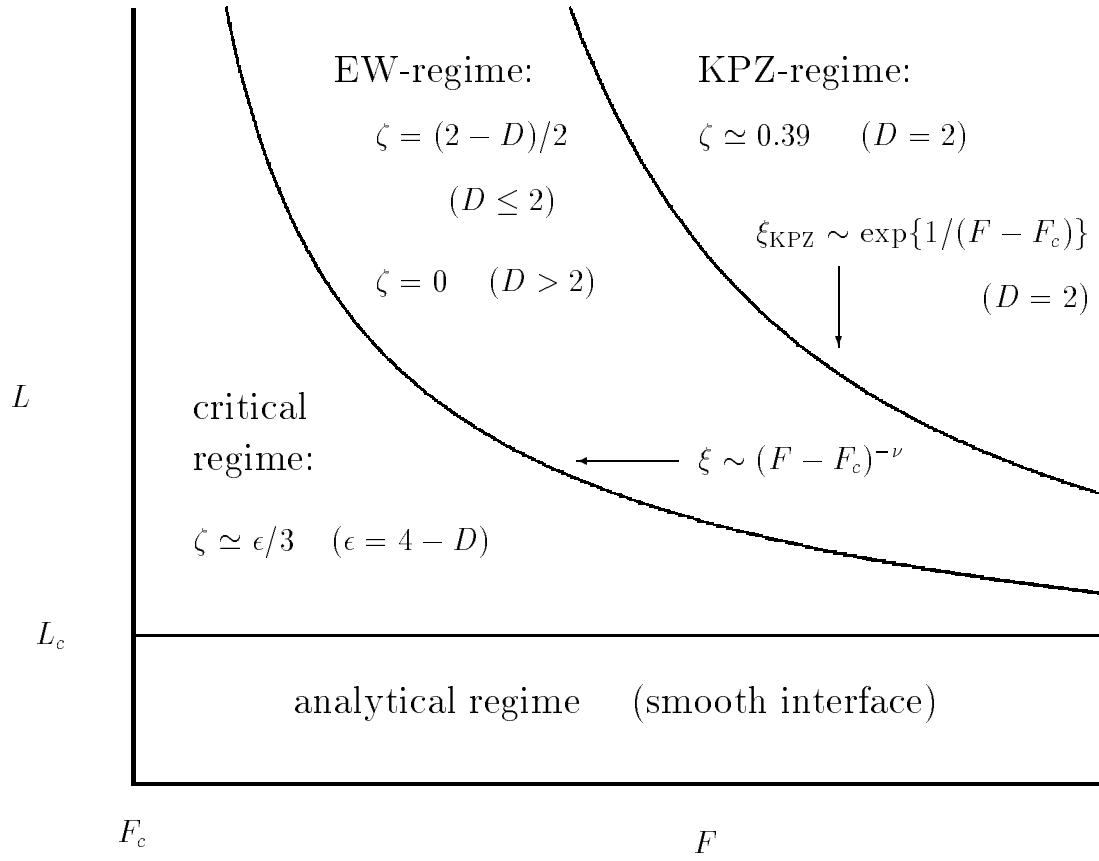


Figure 10

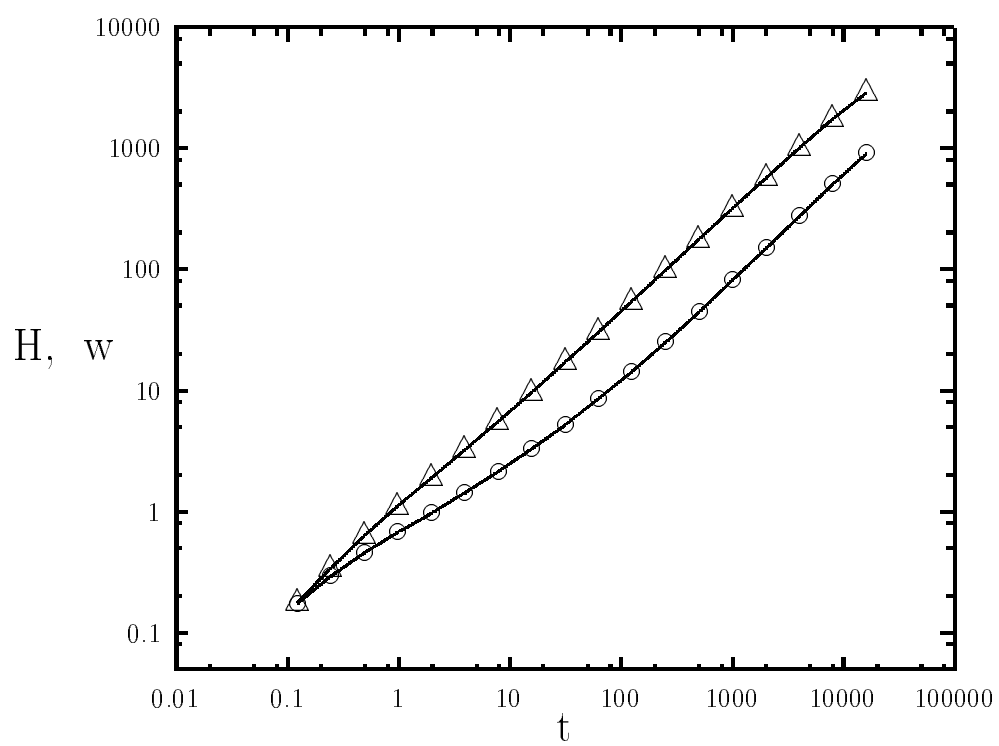




Figure 11

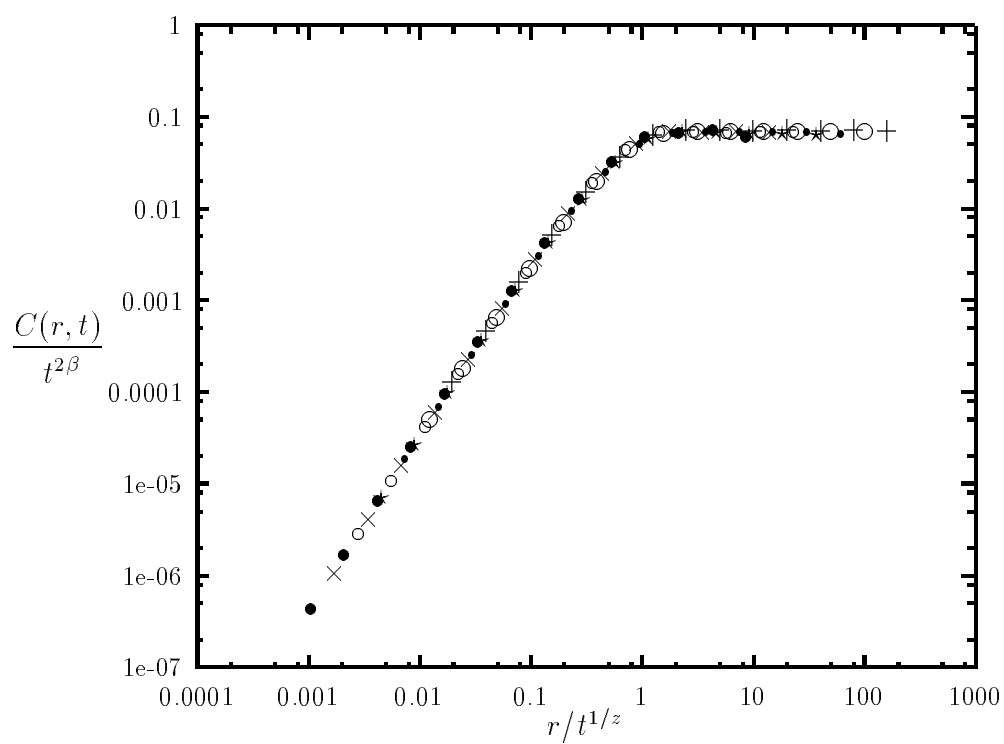


Figure 12

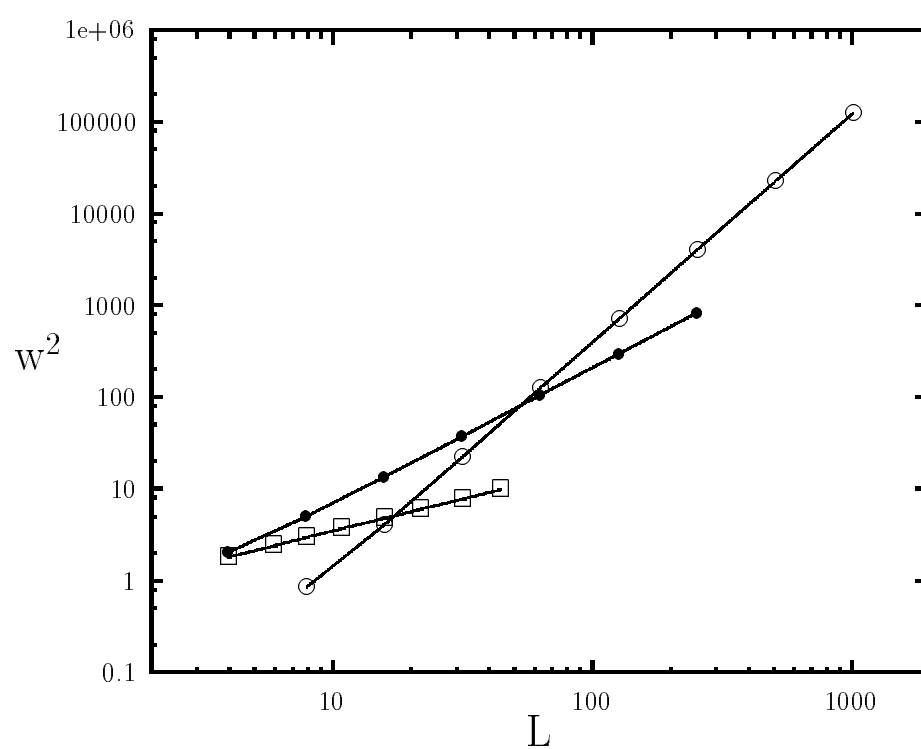


Figure 13

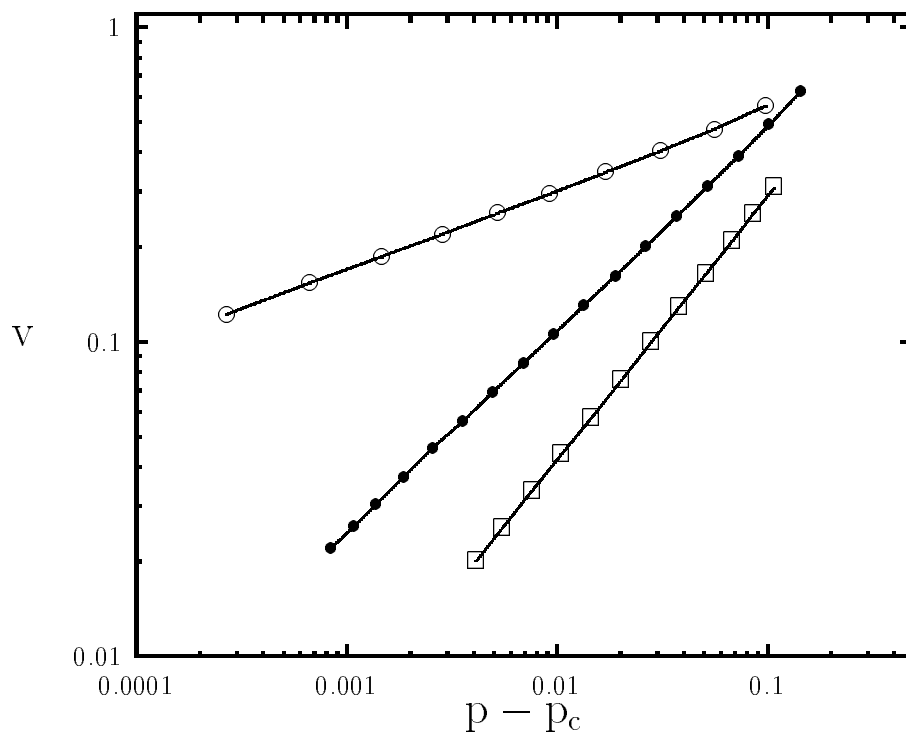
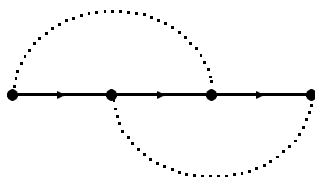
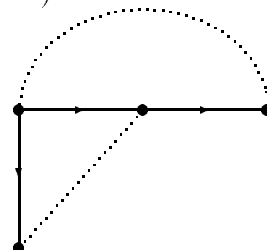


Figure 14

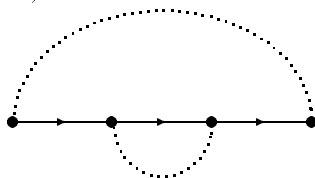
a)



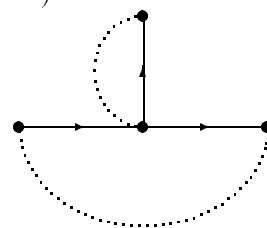
b)



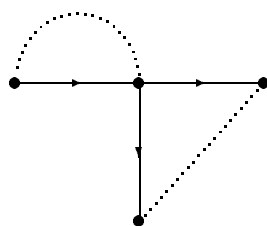
c)



d)



e)



f)

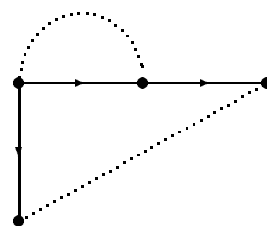
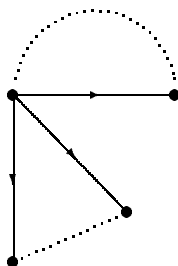
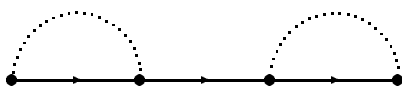


Figure 14

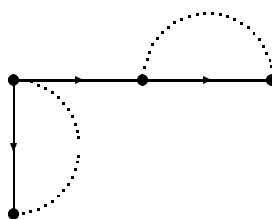
g)



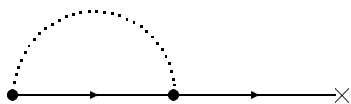
h)



i)



j)



k)

